AGU PUBLICATIONS

JGR

Journal of Geophysical Research: Oceans

RESEARCH ARTICLE

10.1002/2016JC011680

How does Subantarctic Mode Water ventilate the Southern Hemisphere subtropics?

Daniel C. Jones[1], Andrew J. S. Meijers[1], Emily Shuckburgh[1], Jean-Baptiste Sallée[2], Peter Haynes[3], Ewa K. McAufield[1,3], and Matthew R. Mazloff[4]

[1]British Antarctic Survey, NERC, Cambridge, UK, [2]LOCEAN, CNRS, Paris, France, [3]DAMTP, University of Cambridge, Cambridge, UK, [4]Scripps Institution of Oceanography, UCSD, La Jolla, California, USA

Key Points:
- The export of Subantarctic Mode Water into the subtropical thermocline displays significant regional variability
- Export pathways display the relative influence of the subtropical gyres and ACC
- The Eastern Pacific pathway is an especially efficient mode water export route due to boundary current transport

Supporting Information:
- Supporting Information S1
- Movie S1
- Movie S2
- Movie S3
- Movie S4
- Movie S5
- Movie S6
- Movie S7

Correspondence to:
D. C. Jones,
dannes@bas.ac.uk

Citation:
Jones, D. C., A. J. S. Meijers, E. Shuckburgh, J.-B. Sallée, P. Haynes, E. K. McAufield, and M. R. Mazloff (2016), How does Subantarctic Mode Water ventilate the Southern Hemisphere subtropics?, *J. Geophys. Res. Oceans*, *121*, 6558–6582, doi:10.1002/2016JC011680.

Received 26 JAN 2016
Accepted 12 AUG 2016
Accepted article online 18 AUG 2016
Published online 5 SEP 2016
Corrected 4 NOV 2016

This article was corrected on 4 NOV 2016. See the end of the full text for details.

Abstract In several regions north of the Antarctic Circumpolar Current (ACC), deep wintertime convection refreshes pools of weakly stratified subsurface water collectively referred to as Subantarctic Mode Water (SAMW). SAMW ventilates the subtropical thermocline on decadal timescales, providing nutrients for low-latitude productivity and potentially trapping anthropogenic carbon in the deep ocean interior for centuries. In this work, we investigate the spatial structure and timescales of mode water export and associated thermocline ventilation. We use passive tracers in an eddy-permitting, observationally-informed Southern Ocean model to identify the pathways followed by mode waters between their formation regions and the areas where they first enter the subtropics. We find that the pathways followed by the mode water tracers are largely set by the mean geostrophic circulation. Export from the Indian and Central Pacific mode water pools is primarily driven by large-scale gyre circulation, whereas export from the Australian and Atlantic pools is heavily influenced by the ACC. Export from the Eastern Pacific mode water pool is driven by a combination of deep boundary currents and subtropical gyre circulation. More than 50% of each mode water tracer reaches the subtropical thermocline within 50 years, with significant variability between pools. The Eastern Pacific pathway is especially efficient, with roughly 80% entering the subtropical thermocline within 50 years. The time required for 50% of the mode water tracers to leave the Southern Ocean domain varies significantly between mode water pools, from 9 years for the Indian mode water pool to roughly 40 years for the Central Pacific mode water pool.

1. Introduction

Deep winter convection north of the Subantarctic Front (SAF) of the Antarctic Circumpolar Current (ACC) forms pools of highly oxygenated, weakly stratified (i.e., low potential vorticity) subsurface water collectively referred to as Subantarctic Mode Water (SAMW) [*McCartney*, 1977; *Hanawa and Talley*, 2001]. Pools of SAMW are found in each ocean basin, and their temperature/salinity properties vary with longitude. Eastward of the Indian basin, we find progressively colder, fresher, and higher-latitude pools of SAMW, as the formation regions tend to stay just north of the poleward-spiraling SAF [*Hanawa and Talley*, 2001; *Sallée et al.*, 2008a]. SAMW ventilates the Southern Hemisphere thermocline, providing nutrients that support low-latitude productivity and sequestering anthropogenic carbon in the interior ocean [*McNeil et al.*, 2001; *Sloyan and Rintoul*, 2001; *Sarmiento et al.*, 2004; *Sabine et al.*, 2004; *Khatiwala et al.*, 2009; *Iudicone*, 2010; *Talley*, 2013]. Here "ventilation" refers to the detrainment of water and tracers (e.g., CO_2) out of the surface mixed layer into the ocean interior without returning to the mixed layer in subsequent years.

Ventilation is intimately tied up with the formation, circulation, and destruction of water masses [*Robinson and Stommel*, 1959; *Welander*, 1959; *Luyten et al.*, 1983; *Speer and Tziperman*, 1992; *Primeau and Holzer*, 2006; *Liu and Huang*, 2012; *Trossman et al.*, 2012]. In particular, understanding subtropical thermocline ventilation requires a thorough consideration of how SAMW is created, subducted, and exported [*Luyten et al.*, 1983; *Musgrave*, 1990; *Sloyan and Rintoul*, 2001; *Sallée et al.*, 2010]. SAMW is thought to be sourced by upwelled Pacific Deep Water (PDW) and Indian Deep Water (IDW) that is advected into the SAMW formation regions, where seasonal deep convection refreshes the subsurface SAMW pools [*Speer et al.*, 2000; *Lumpkin and Speer*, 2007; *Talley*, 2008]. *Downes et al.* [2011] further hypothesize that Upper Circumpolar Deep Water (UCDW) and Antarctic Intermediate Water (AAIW) may be converted into SAMW by surface buoyancy fluxes.

Observationally-constrained model estimates suggest that the spatially integrated and time-averaged SAMW formation rate in the Southern Ocean surface layer is 7.9 Sv by air-sea buoyancy fluxes and 8.8 Sv by diapycnal mixing [*Cerovečki and Mazloff*, 2015].

The subduction of SAMW occurs in relatively narrow regions, driven by lateral induction, eddy-induced transport, and mean flow [*Karsten and Marshall*, 2002; *Sallée et al*., 2008b,2010; *Sallée and Rintoul*, 2011; *Sallée et al*., 2012]. Once SAMW has been subducted out of the formation regions, some fraction of it ultimately ends up in the deep interior ocean away from the mixed layer, where it is no longer in seasonal contact with the atmosphere. Together, SAMW and AAIW contribute 8 Sv (1 Sv $= 10^6$ m^3/s) to the equatorward volume flux across 30°S, with 6 Sv into the Indian and Pacific basins and 2 Sv into the Atlantic [*Talley*, 2008, 2013]. This is a significant fraction of the 13 Sv total volume flux that crosses 30°S in the upper cell of the global meridional overturning circulation [*Talley*, 2013]. Small changes in the properties of SAMW and AAIW can thus have a disproportionate effect on subtropical thermocline waters. Note that the equatorward volume flux is smaller than its formation rate due to recirculation in the gyres [*Cerovečki and Mazloff*, 2015].

The export pathways associated with distinct SAMW pools, as revealed by subsurface potential vorticity minima, display notable spatial variability that can only be fully captured by three-dimensional representations of ocean circulation [*Sallée et al*., 2010; *Herraiz-Borreguero and Rintoul*, 2011]. The destruction of SAMW by diapycnal mixing also displays significant regional variation [*Cerovečki et al*., 2013]. These regional differences are relevant for thermocline ventilation, the supply of nutrients to low-latitudes, and carbon sequestration [*Sarmiento et al*., 2004; *Sabine et al*., 2004; *Khatiwala et al*., 2009; *Ito et al*., 2010]. The export of SAMW into the interior thermocline is not perfectly efficient, nor is it instantaneous; some fraction of subducted SAMW may interact with the mixed layer well after it has initially been subducted. Although recent observational studies have found patterns of potential vorticity and anthropogenic carbon that highlight the broad structure of several mode water export pathways, questions about the export timescales and efficiency of export from various mode water pools remain [*Sallée et al*., 2010; *Herraiz-Borreguero and Rintoul*, 2011; *Sallée and Rintoul*, 2011; *Sallée et al*., 2012]. In this context, export from a mode water pool is "efficient" if a large fraction of tracer that is initialized in that pool ultimately ends up in the subtropical thermocline.

In this work, we examine the transport of SAMW from selected formation regions to where it ventilates the subtropical thermocline. We are interested in (1) following the SAMW after it is formed up until it enters the subtropics and (2) establishing the timescales and relative "efficiency" of the various SAMW export pathways. By the metrics used in this work, SAMW formed in the Southeast Pacific is especially efficient at ventilating the subtropical thermocline. We show that mode waters formed in the Indian basin and Central Pacific are dominated by gyre dynamics, and mode waters formed in the Eastern Pacific and Atlantic basins are more heavily influenced by the ACC. We identify broad export pathways for each pool, estimate SAMW export and decay timescales, and identify the regions where the mode water tracers ultimately enter the subtropics.

2. Model Setup and Experiment Design

In order to examine the transport from selected mode water formation regions to the subtropical thermocline, we carry out a set of numerical passive tracer advection experiments. The passive tracers are initialized in five mode water pools, defined using a combination of potential vorticity, potential density, and position based criteria (see section 2.5), and advected for 50 years. A sponge layer, active near the northern boundary of the model domain (24.7–26.5 °S), effectively absorbs tracers by relaxing the tracer concentration field to zero with a 6 h restoring timescale. Our simulations follow single "pulses" of mode water from each formation region to where they first enter the subtropics. We allow the tracer to enter and exit the mixed layer throughout the experiment, since we are interested in following parcels that start as mode water, including those parcels that are heavily influenced by the mixed layer and mixing with other water masses. The tracers gradually lose their mode water characteristics as they are advected, but we refer to the tracers as "mode water tracers" in reference to where they are initialized.

2.1. The Southern Ocean State Estimate (SOSE)

At minimum, numerical tracer experiments must be driven by a velocity field. Experiments can be further constrained by using temperature, salinity, and associated mixing/convection fields, which may be used in

mixing parameterization schemes. The Southern Ocean State Estimate (SOSE) offers one such set of fields [*Mazloff et al*., 2010]. SOSE is a collection of state estimate products that are constructed by bringing a numerical ocean circulation model (MITgcm) into consistency with a suite of available observations, including data from Argo floats, satellite altimetry, and hydrographic profiles. SOSE approaches consistency by iteratively reducing a measure of disagreement between the model and observations using an adjoint method [*Mazloff et al*., 2010]. The adjoint method is used to map out how the initial conditions and the surface forcing (e.g., wind stress, atmospheric temperature) can be perturbed to reduce the disagreement between the model and observations over the length of the simulation. The result is a physically realistic estimate of the state of the ocean, as well as a set of initial conditions and surface forcings that have been optimized to produce the best agreement between ocean observations and the model state. Due in part to the computationally intensive nature of the 4D-Var optimization process and the sparsity of multidecadal observational data in the Southern Ocean, the SOSE products typically only cover a few years (at present, the available periods are 2005–2007, 2008–2010, and 2005–2010).

2.2. Offline Tracer Advection: A Potential Bias

One approach for driving a numerical tracer experiment is to use the SOSE ocean velocity and hydrography files on repeat, looping the same multiyear period over and over again. In this approach, the tracer advection equations are solved "offline," i.e., the velocity and hydrography are read in as inputs to the tracer advection equation as opposed to being explicitly calculated alongside the tracer concentrations. This offline approach works well for many applications, especially for studies that fall within the 3 or 6 year range of the SOSE products. However, the ventilation of the subtropics via Southern Ocean mode water pools is a decadal-to-centennial scale process [*Primeau and Holzer*, 2006; *Trossman et al*., 2012]. Since the ocean state may drift over any given 3 or 6 year period, tracers simulated over many decades can experience rapid "jumps" each period as the physical fields transition from the end of the forcing record to the beginning (e.g., from the end of 2009 to the start of 2007). Most offline tracer advection setups use linear interpolation to transition between the discrete velocity and temperature fields used as inputs, which helps to minimize (but does not completely remove) the discontinuous "jump" between the end of one forcing file period and the start of another. These jumps can introduce spurious vertical mixing in the tracer fields as the hydrography rapidly shifts in an artificial fashion, distorting the vertical distribution of the tracers. The impact of these jumps on tracer fields will be further explored in an upcoming companion paper. For this paper, we will use an alternative strategy for driving the tracer fields, described below.

2.3. Our Approach: Online Tracer Advection

In this work, we use an alternative to the "offline" approach in which we explicitly solve for the model dynamics (e.g., velocity, potential temperature, salinity) and the passive tracer fields simultaneously. We will call this alternative the "online" approach. The "online" approach is more computationally expensive than the "offline" method and may be subject to some drift during model spin-up, but it does not rely on linear interpolation between discrete velocity input fields and does not suffer from the discontinuous jump problem described in the previous section. The online approach also requires a full model setup, i.e., the setup must be able to solve for the dynamics as well as integrate the advection-diffusion equation for passive tracers. Multidecadal online runs of eddy-permitting regional models are feasible on modern, high-performance computing platforms.

2.4. BASSOON

Here we describe the online modeling framework used in this work, called the **B**ritish **A**ntarctic **S**urvey/**SO**SE **ON**line model, or BASSOON. BASSOON is a configuration of the Massachusetts Institute of Technology general circulation model (MITgcm) that is closely related to the numerical model setup used to generate the SOSE products [*Marshall et al*., 1997a,1997b; *Mazloff et al*., 2010]. Although the BASSOON setup is "realistic" in terms of its bathymetry and forcing, it should not be used as a future projection of the current ocean state. Instead, it is an eddy-permitting representation of quasi-steady Southern Ocean circulation that is broadly similar to the modern ocean.

To construct BASSOON, we started with the MITgcm setup used to generate SOSE for the years 2007–2009. This setup consists of (i) a set of initial conditions for temperature, salinity, and velocity, (ii) surface forcing fields (e.g., zonal and meridional winds) and freshwater input from the continents, (iii) bathymetry, (iv) the configuration of the discrete model grid, and (v) a set of physical parameters (e.g., viscosity). Note that the

Table 1. Parameters Used in the Online Model Setup

Advection Scheme	Third-Order Direct Space Time
Isopycnal diffusivity	10 m^2/s
Vertical diffusivity	10^{-5} m^2/s
Biharmonic horizontal diffusivity	10^{10} m^4/s
Vertical viscosity	10^{-4} m^2/s
Horizontal viscosity	10 m^2/s
Biharmonic horizontal viscosity	10^{10} m^4/s
Linear bottom drag	10^{-3} m^2/s

initial conditions and surface forcing fields have been optimized using the 4D-Var process as described in section 2.1. The BASSOON setup was kept as close as possible to the model setup used to generate SOSE, which is a model with 1/6° horizontal resolution, 42 vertical levels of varying thickness (i.e., thinner surface layers and thicker deep ocean layers), and a 900 s time step. Additional model parameters for diffusivity, viscosity, and bottom drag are listed in Table 1. We use biharmonic horizontal diffusivity and viscosity, harmonic horizontal viscosity, and harmonic vertical diffusivity and viscosity. Vertical mixing is represented by the *K*-profile parameterization (KPP) scheme, which in our setup mixes both momentum and tracers near the surface [*Large et al*., 1994]. For more details, see *Mazloff et al*. [2010]. The changes between the SOSE setup and BASSOON are described below.

2.4.1. Surface Forcing

The 4D-Var optimization process used to generate SOSE perturbs a set of 6 hourly ERA-Interim atmospheric forcing fields (i.e., shortwave and longwave radiation, surface pressure, precipitation, specific humidity at 2 m above the sea surface, air temperature at 2 m, and both zonal and meridional winds at 10 m) in order to minimize the mismatch between the ocean model state and ocean observations (see section 2.1). The results of this optimization process are available on the SOSE website (http://sose.ucsd.edu/).

To construct a suitable set of surface forcing fields for conducting multidecadal BASSOON runs, we start with the 6 hourly SOSE optimized fields for 2007–2009 (iteration 60) and remove the 3 year linear trend at each location in longitude/latitude. The resulting fields have the same variability as the SOSE-adjusted fields on time scales shorter than 3 years. Some inter-annual variability persists, and the impact of this inter-annual variability can be seen in the surface fields (e.g., sea ice volume, not shown). The de-trended 3 year surface forcing fields are looped indefinitely, which allows for multidecadal runs.

2.4.2. Subgrid Scale Parameterization

Hallberg [2013] demonstrated that eddy mixing parameterization schemes can suppress resolved eddies, e.g., by artificially smoothing out gradients associated with resolved mesoscale features. Like the SOSE-generating setup, BASSOON does not use any subgrid scale eddy parameterizations for lateral mixing (both setups use biharmonic horizontal diffusivity and viscosity, harmonic horizontal viscosity, and harmonic vertical diffusivity and viscosity). In the regions most relevant to our study (i.e., north of the ACC), the first baroclinic deformation radius is of order 20 to 50 km away from topographic shelves, which is roughly 1.0 to 2.5 horizontal grid box widths; larger mesoscale features (typically of order 100 km, 3–5 times the deformation radius in the midlatitudes) are fully resolved and are not artificially suppressed (see supporting information) [*Chelton et al*., 1998; *Hallberg*, 2013]. In shallow seas (e.g., the Patagonian Shelf, Campbell Plateau, along the Australian and South African coasts), the first baroclinic deformation radius is less than 1 km and is not resolved, so eddy-driven tracer mixing in these areas may be biased toward weak values. The resulting mesoscale eddy variability of the 1/6° SOSE configuration, on which BASSOON is based, compares favorably with the AVISO optimally interpolated satellite altimetry product [*Mazloff et al*., 2010, Figure 1]. The agreement is weaker in shallow seas.

2.4.3. Sea Ice

Many models with a Southern Ocean are prone to the formation of extremely large ($>10^5$ km^2) open-ocean sensible-heat polynyas that are associated with unrealistically deep mixed layers and the destruction of stable salt stratification [*Timmermann and Beckmann*, 2004; *Timmermann and Losch*, 2005; *Heuzé et al*., 2013; *Stossel et al*., 2015; *Kjellsson et al*., 2015]. In order to prevent model drift and to discourage the formation of large-scale polynyas and the onset of the associated runaway positive feedback loop, we used surface salt restoring to monthly mean SOSE climatology (from the 2005–2010 product, iteration 100) with a 30 day relaxation timescale. Much longer relaxation timescales (e.g., 4 months) do not prevent the formation of polynyas and the subsequent runaway vertical mixing/ice melt positive feedback loop.

2.4.4. Validation

BASSOON is allowed to spin-up for 10 years, after which we find that most of the adjustment in the relevant depths for mode waters (200–1000 m) has occurred. The deep ocean will continue to adjust well after the spin-up period, which is seen as a slight change in the density structure. The northern boundary is restored

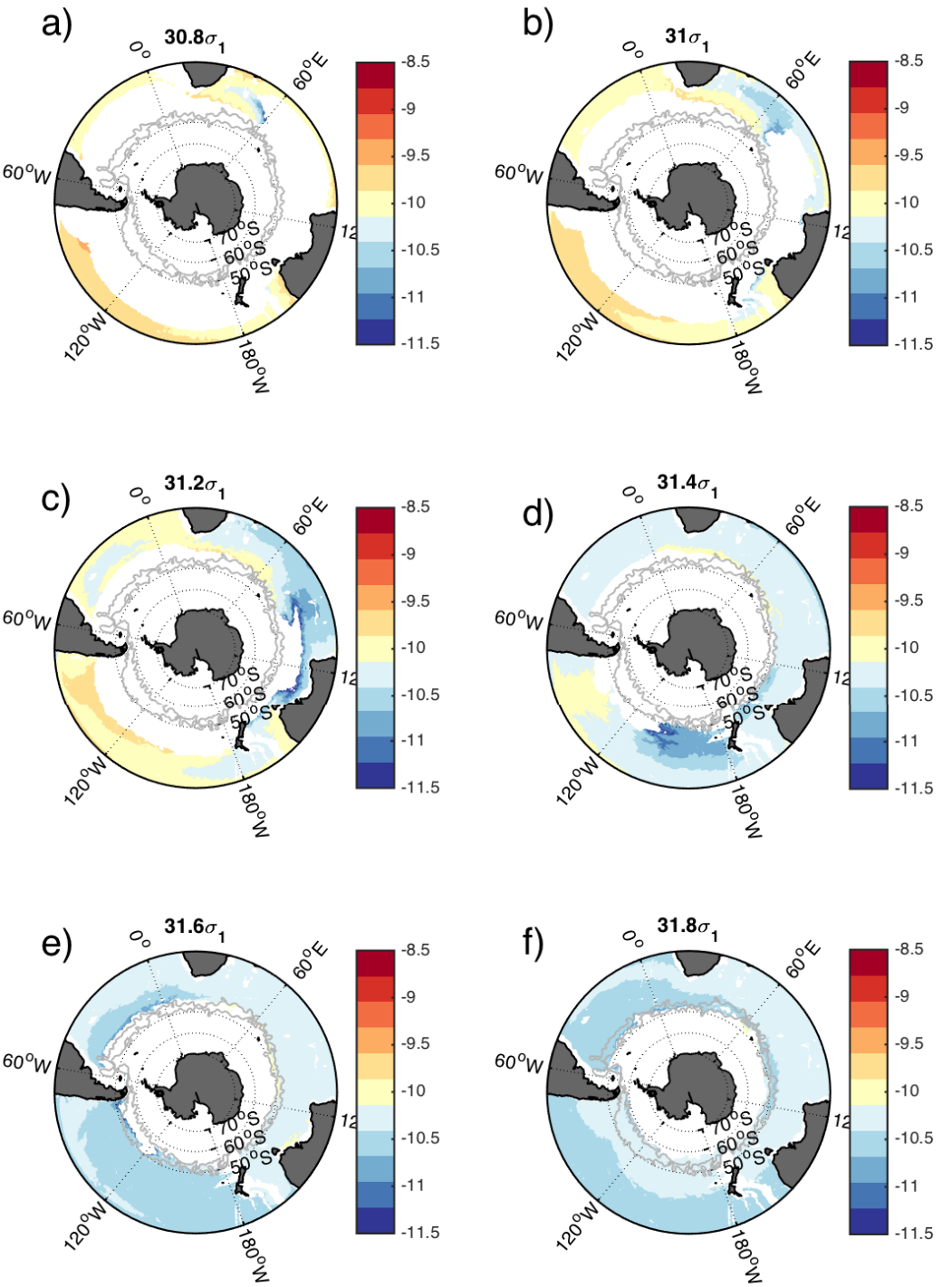

Figure 1. Annual mean potential vorticity (1/ms, $\log_{10}$ scale) in BASSOON after the 10 year spin-up period, projected onto σ_1 potential density surfaces (kg/m^3). The two solid lines are the 90 Sv and 130 Sv contours of the annual mean barotropic streamfunction after the 10 year spin-up period (1 Sv = 10^6 m^3/s).

to a prescribed profile, which helps to prevent excessive long-term drift. The dynamics and seasonality of BASSOON are broadly consistent with the observed state of the Southern Ocean. The mean transport of the Antarctic Circumpolar Current over the 50 year simulation period is 133 Sv (1 Sv = 10^6 m^3 s^{-1}), with a standard deviation of 4 Sv. This compares well with the observed mean transport of 134 ±13 Sv [*Whitworth*, 1983; *Whitworth and Peterson*, 1985; *Rintoul et al.*, 2001; *Thompson*, 2008]. There is a linear trend of −0.1 Sv/yr, which reflects the longer term shift in water mass location and properties (i.e., the model is only

quasi-stationary). The sea ice area (i.e., the integral of sea ice concentration) has a mean value of 1.0×10^7 km^2 and a large seasonal variability with amplitude 1.6×10^7 km^2, which compares very well with observational and model estimates [*Holland et al*., 2014; *Comiso*, 2015]. There is no significant linear trend in sea ice area or volume, which is largely due to the strong sea surface salinity restoring.

2.4.5. Model Setup Caveats

BASSOON is an ocean model that is designed to remain in a quasi-steady state for several decades. This is obviously an idealization of the real ocean, which of course does not necessarily stay in a quasi-steady state on decadal timescales. It would be useful to investigate the effects of changing surface forcing patterns (e.g., changes in SAM or ENSO) on the structure of the mode water export pathways. Due to both the regional setup and the online nature of our runs, we can only run tracer experiments for a few decades before the "re-entrance" problem (e.g., reentrance of mode water due to gyre circulation) becomes relevant. Although the primary focus of our work is on the initial export of mode waters out of the model domain, it would be instructive to run a complementary set of experiments in a global model.

2.4.6. Potential Vorticity Structure

Since mode waters are weakly stratified, one can use anomalously low values of potential vorticity as a proxy for mode waters. The interior ocean potential vorticity structure in the spun-up BASSOON state compares favorably (see Figure 1) with observationally-derived climatological PV structure in sufficient detail for our large-scale study [*Sallée et al*., 2010; *Herraiz-Borreguero and Rintoul*, 2011]. In the Indian Ocean and south of Australia, a large mode water pool extends from just north of the Antarctic Circumpolar Current to the northern edge of the model, sweeping westward in a broad pattern (Figures 1b and 1c). The PV gradually increases along this northwestward track, as the mode water mixes with surrounding water masses on its way out of the model domain. A similar westward-spreading mode water pool is found in the Central Pacific Ocean, north of the ACC (Figure 1d). The Central Pacific pool spreads westward up to the New Zealand coast, where it splits into a northward branch that leaves the Southern Ocean and a westward branch that spreads south of Australia. In the Eastern Pacific, a mode water pool and export path are found close to the southern tip of South America, spreading rapidly northward and westward (Figure 1e). This pool is situated close to an important region of formation and export of Antarctic Intermediate Water (AAIW), which sits slightly deeper than the mode water (not shown). Finally, in the Atlantic sector, we find a pool of mode water within the contours of the Antarctic Circumpolar Current (Figure 1f). This Atlantic mode water pool is thought to be largely composed of mode water that formed upstream of Drake Passage in a region of deep mixed layers and advected onto the Scotia Sea by the intense zonal flow of the ACC [*Sallée et al*., 2010].

In Figure 2, we plot three cuts of annual mean potential vorticity after the 10 year spin-up period in density/depth and latitude. The mode water pools sit below the surface layer, which refreshes the mode water pools in winter and re-stratifies in the spring and summer, isolating the mode water pools from the surface. The mode water pools in the cuts are located between 200 and 500 m, north of the steeply sloping density surfaces of the ACC. The cuts also reveal weakly stratified waters south of 50°S, as well as everywhere below roughly 1500 m [*Talley*, 2013]. We find that the position of the density surfaces changes little after the 10 year spin-up due to the strong restoring conditions at the surface and northern boundary.

2.5. Experiment Design

After the 10 year spin-up period, we identify several mode water pools using a combination of criteria involving potential vorticity, potential density referenced to 1000 dbar (σ_1), latitude, and longitude (see Figure 3 and Table 2). The initial sizes of the passive tracer patches are small, since the patches must satisfy all of the criteria given in Table 2 (except for the transport, which is diagnosed). The tracers in the Indian and Pacific basins are initialized just north of areas of deep winter mixed layers, which is barely downstream of the mode water formation regions. The Australian tracer location is north of the ACC and just south of a patch of deep winter mixed layers around Tasmania. The Atlantic tracer is not especially close to deep mixed layer, indicating that this mode water pool may be formed and refreshed from upstream of Drake Passage or the Falkland Islands. The Indian, Australian, and Central Pacific tracers are initialized in more "gyre like" contours, and the Eastern Pacific and Atlantic are initialized on more "ACC like" contours.

We initialize tracer in the locations shown in Figure 3, effectively "tagging" several SAMW pools. The tracers are initialized on 1 January, i.e., in Austral summer when the mixed layers are relatively shallow. We advect

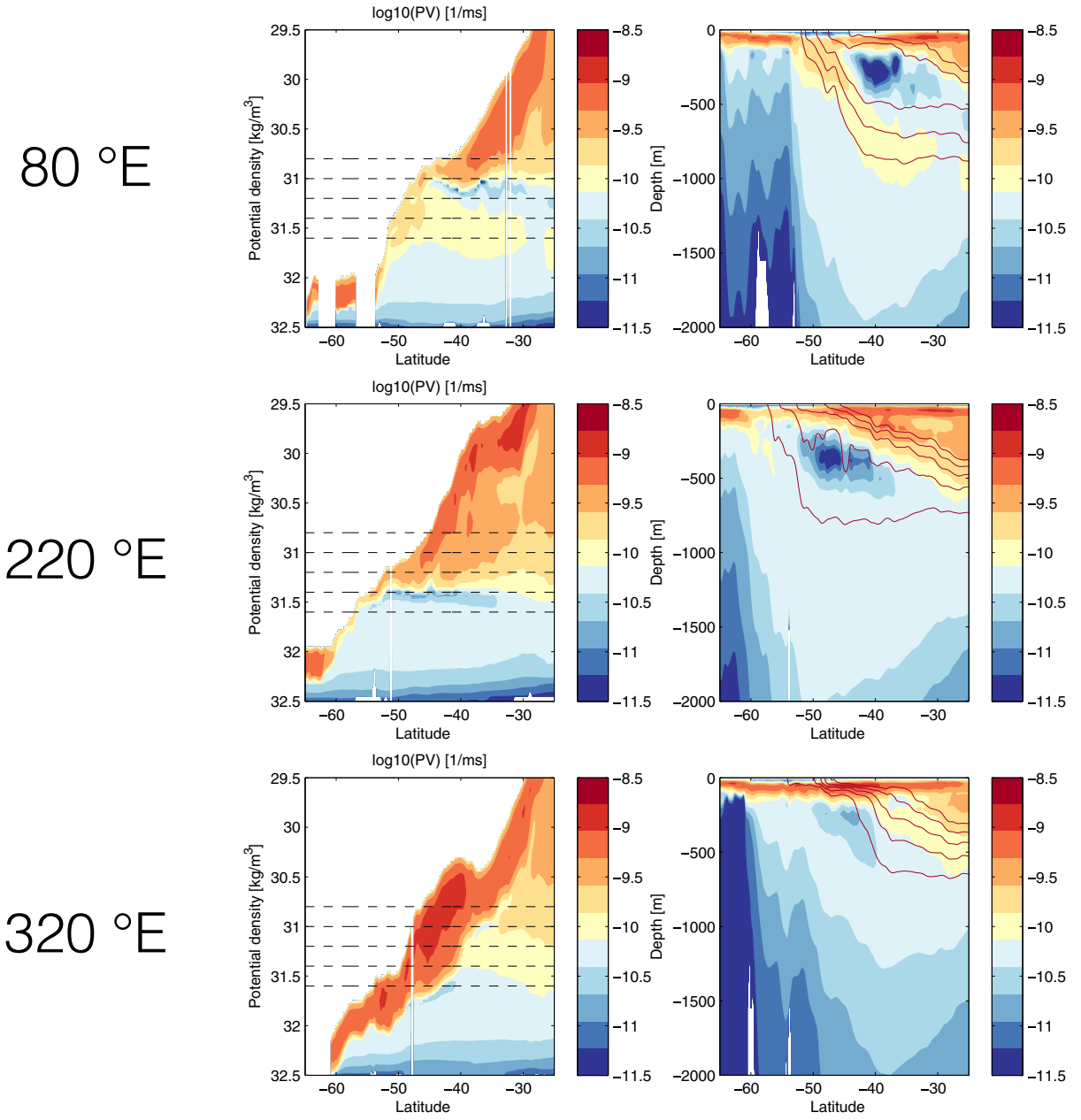

Figure 2. (left column) Density/latitude cuts of annual mean potential vorticity (1/ms, $\log_{10}$ scale) in BASSOON after the 10 year spin-up period, and (right column) depth/latitude cuts of the same quantity. Values are shown at three different longitudes, 80 °E, 220 °E, and 320 °E. The dashed lines in the left column correspond to the five density surfaces shown as solid lines in the right column.

the tracer, temperature, and salinity using a third-order direct space-time scheme for consistency with how temperature and salinity are advected in the SOSE model setup of *Mazloff et al.* [2010]. After the initial 10 year model spin-up period, tracers are initialized and then advected for an additional 50 years. The model tracer output consists of five different sets of three-dimensional tracer concentration fields (one set of fields for each tracer experiment) and several physical/model fields (e.g., temperature, salinity, stratification $d\rho/dz$). We place a sponge layer between 26.5 °S and the northern edge of the model at 24.7 °S with a 6 h *e*-folding timescale, such that any tracer that reaches this sponge layer is rapidly removed from the model domain. We focus our attention on how mode waters first make their entrance to the subtropics (i.e., crossing 26.5 °S and getting absorbed by the sponge layer). In a global ocean domain, mode waters may of course cross this arbitrary dividing line many times. We save this "re-entrance problem" for future study.

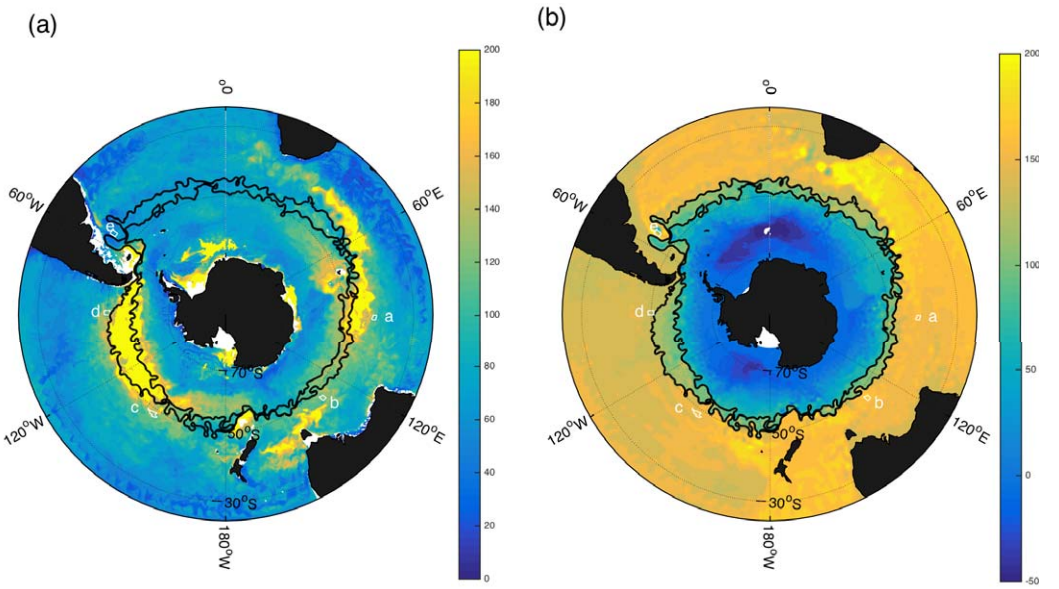

Figure 3. The size and placement of the initial tracer patches, indicated by white contours and letters. The color scales show (a) JJA mixed layer depth [m], calculated by integrating the stratification $d\rho/dz$ from the surface down to z_{ml}, where $\Delta\rho=\rho(z_{ml})-\rho(z=0)=0.03$ kg/m^3, and (b) annual mean vertically integrated transport (Sv). The two solid lines are the 90 Sv and 130 Sv contours of the annual mean barotropic streamfunction after the 10 year spin-up period.

2.6. Vertical Spreading

For consistency with temperature and salinity mixing in the SOSE setup, we impose (1) a vertical diffusion coefficient of $K_z=10^{-5}$ m^{2}s^{-1} and (2) additional vertical mixing due to mixed layer convection via KPP. In order to better understand the vertical spreading of the tracers, we fit each tracer distribution about its center of mass in longitude and latitude to a Gaussian profile in density, i.e., $f(\sigma_1)=A\exp\left[-(\sigma_1-b)^2/c^2\right]$, where A, b, and c are fitting parameters. The tracers do spread out quickly in density space (i.e., A and c change rapidly) due in part to the action of KPP, but the tracer center of mass stays on the same density surface (i.e., b_1 changes by $\ll 1\%$ over the first 4 years of the experiment). The results of the fitting and a few animations of how the tracer spreads in the vertical can be found in the supporting information. The tracers are allowed to interact with the vertical mixing parameterization scheme (i.e., KPP), which explains some of the observed vertical spreading.

2.7. Tracer-Weighted Diagnostics

Tracer-weighted properties help quantify when and where changes in water mass properties take place during tracer transport [e.g., *Qu et al.*, 2013; *Wang et al.*, 2014]. For instance, tracer-weighted potential temperature $\bar{\theta}$ can be used as a proxy for tracer heat content:

$$\overline{\theta(t)}=\frac{\int\phi\theta dV}{\int\phi dV}, \tag{1}$$

where ϕ is a tracer field and the integral is over a volume V [*Wang et al.*, 2014]. The time series $\overline{\theta(t)}$ gives us information on how the tracer heat content changes as the tracer (which represents a particular collection

Table 2. Characteristics of Tracer Initial Condition Sites[a]

Basin	Lat (N)	Lon (E)	z (m)	σ_0 (kg/m^3)	σ_1 (kg/m^3)	Log10(PV) (1/ms)	Ψ (Sv)
Indian	[−42, −40]	[90, 92]	[300, 400]	[26.5, 26.7]	[31.0, 31.2]	[−12.5, −11.0]	186
Australian	[−48, −46]	[130, 132]	[400, 500]	[26.7, 26.9]	[31.2, 31.4]	[−12.5, −11.0]	180
C. Pacific	[−50, −46]	[200, 250]	[150, 600]	[26.7, 26.9]	[31.2, 31.4]	(−∞,−11.0]	186
E. Pacific	[−51, −49]	[270, 272]	[300, 500]	[26.9, 27.0]	[31.4, 31.6]	(−∞,−11.0]	137
Atlantic	[−45, −43]	[305, 307]	[300, 500]	[27.0, 27.2]	[31.6, 31.8]	[−11.5, −10.25]	196

[a]σ_1 is used for selection; σ_0 and Ψ are shown only for reference.

of water mass parcels) mixes with other water masses and interacts with the mixed layer. Here we use tracer-weighted properties to better understand how mode water is altered as it makes its way from the formation regions to the subtropical thermocline.

In this paper, the interpretation of tracer-weighted properties (e.g., potential temperature, salinity) is complicated by the fact that tracer is removed from the northern domain of the model. That is, the removal of tracer by the sponge layer introduces bias into tracer-weighted properties. Using a global ocean domain would resolve this problem, but using a global domain is not always feasible or desirable. We need a method for estimating the uncertainty introduced by tracer removal in a regional ocean model with a sponge layer at the northern edge. Below, we introduce one such method.

2.7.1. Estimating Uncertainty in Tracer-Weighted Properties

We have a tracer field ϕ, a removal field R (e.g., the cumulative removal histogram representing the action of the sponge layer near the northern edge of the model domain), and various physical fields f (e.g. potential temperature, salinity, depth, potential vorticity). In general, tracer-weighted properties are given by volume integrals over the global ocean domain:

$$\bar{f} = \frac{\int_{global} \phi f dV}{\int_{global} \phi dV} = \frac{\int_{global} \phi f dV}{\Phi_{global}}, \tag{2}$$

which can be split into a volume integral inside the model domain ("in") and a volume integral outside the model domain ("out"),

$$\bar{f} = \frac{1}{\Phi_{global}} \left(\int_{in} \phi f dV + \int_{out} \phi f dV \right) = \overline{f_{in}} + \overline{f_{out}}. \tag{3}$$

We can calculate $\overline{f_{in}}$, but we cannot explicitly calculate the second term, as it lies outside of our model domain by definition. Instead, we define $\overline{f_{out}}$ as an error term weighted by the total amount of tracer contained in the model domain:

$$\overline{f_{out}} = (f_0 \pm \Delta f) \left(1 - \frac{\Phi_{in}}{\Phi_{global}} \right), \tag{4}$$

where $\Phi_{in} = \int_{in} \phi dV$ and $\Phi_{global} = \int_{global} \phi dV$. At the beginning of the simulation, all of the tracer is in the model domain and the uncertainty term vanishes. As tracer leaves the model domain, $\bar{f}$ asymptotes to $f_0 \pm \Delta f$. So how should we choose f_0 and Δf? We can interpret Δf as the removal-weighted standard deviation at the northern boundary:

$$(\Delta f)^2 = \frac{1}{\int_{nb} R dV} \int_{nb} (f - f_0)^2 R dV, \tag{5}$$

where f_0 is the removal-weighted expected value:

$$f_0 = \frac{1}{\int_{nb} R dV} \int_{nb} R f dV. \tag{6}$$

This method effectively "freezes" the value of f as the tracer is removed from the domain, within an error term determined by the spread of f about f_0 at the northern edge of the model domain.

2.7.2. Tracer Moments and Eccentricity

Moments of the tracer distribution, which are useful for characterizing the shape and properties of the tracer patches, are given by:

$$M_{pqr} = \sum_{i,j,k} x_i^p y_j^q z_k^r \phi(x_i, y_j, z_k) \Delta V, \tag{7}$$

where ϕ is the tracer concentration and $\Delta V = \Delta x \Delta y \Delta z$ is the volume element. Central moments of the tracer distribution are then:

$$\mu_{pqr}=\sum_{i,j,k}(x_i-\bar{x})^p(y_j-\bar{y})^q(z_k-\bar{z})^r\phi(x_i,y_j,z_k)\Delta V, \tag{8}$$

where $(\bar{x},\bar{y},\bar{z})=(M_{100},M_{010},M_{001})$. For a two-dimensional tracer distribution (e.g., a column sum, $r=0$), the covariance matrix C is:

$$C[\phi(x,y)]=\frac{1}{\mu_{00}}\begin{bmatrix}\mu_{20} & \mu_{11}\\ \mu_{11} & \mu_{02}\end{bmatrix}. \tag{9}$$

The eccentricity e of the tracer distribution is determined by the eigenvalues λ_1 and λ_2 of the covariance matrix C:

$$e=\sqrt{1-\frac{\lambda_2}{\lambda_1}}. \tag{10}$$

3. Highlighting Mode Water Export Pathways

In our numerical experiments, five mode water tracers track the transport of SAMW after it has been formed by deep wintertime convection. Some of these pathways ultimately involve export out of the Southern Ocean, which in our setup is represented by a tracer-removing sponge at the northern boundary of our model domain (i.e., 24.7–26.5 °S). Since the tracers are removed at the northern boundary, our model setup does not capture the possible re-entrance of mode water back into the Southern Ocean domain once it crosses 26.5 °S. However, our setup does feature mesoscale eddies, deep convection (via KPP mixing), and decadal timescales. As mode water tracers are advected, we diagnose tracer mixing with the surrounding water masses and with the mixed layer, since we are interested in following the full export history of water parcels (up to removal between 24.7 and 26.5 °S) that are formed in the chosen mode water pools. Parcels that are formed as mode water may come into contact with the surface more than once during their export.

3.1. Horizontal Structure of Export Pathways

In this section, we examine the lateral structure of the mode water tracer distributions. We analyze the spatial structure of the export pathways using depth-integrated cumulative tracer amounts in each grid column over the 50 year simulation (Figure 4), and we use the Cunningham streamfunction to analyze geostrophic circulation on isopycnals (Figure 5) [*Cunningham*, 2000; *McDougall*, 1989]. Note that this streamfunction is only an approximation to the geostrophic flow on density surfaces, as the exact streamfunction on an isopycnal does not exist [*Sallée et al.*, 2010]. Broadly speaking, the potential patterns reveal several possible mode water export routes (i.e., contours that intersect the northern boundary of the domain) that are consistent with those reported in *Sallée et al.* [2010]. In Figure 6, we plot time series of the total amount of tracer between 200 - 1300 m. The basin edges defined somewhat arbitrarily as Indian (20E, 146E), Pacific (146E, 60W), and Atlantic (60W, 20E). Below, we discuss each tracer experiment in turn.

3.1.1. Indian Mode Water

Over the course of the 50 year experiment, the bulk of the tracer initialized in the Indian Subantarctic Mode Water pool (i.e., initialization site "a" in Figure 3) stays confined to the Indian basin or is removed by the sponge layer in the Indian sector. The broad structure of this export pathway is influenced by the mean circulation of the subtropical Indian gyre (see Figures 5b and 5c). The total concentration between 200 and 1300 m drops by 21% in the first year due to vertical mixing between the surface ocean and the mode water pool (Figure 6a). The tracer is initialized in a mode water pool that is annually de-stratified by deep winter mixed layers, so we expect some of the tracer to get "mixed out" of the mode water pool in the first winter following the initialization of the tracer (it may also be "mixed back in" in following winter deep-convection events). Over the first 5 years after initialization, the patch spreads out primarily in longitude due to the influence of the ACC; the eccentricity of the tracer patch, calculated from the eigenvalues of the covariance matrix of the tracer distribution (equation (10)), increases from 0.8 to just over 1.0. As the tracer spreads out in latitude, its southern end is sheared further by circumpolar flow, but only a vanishingly small fraction of the tracer ends up poleward of the Subantarctic Front. After the first 5 years, the total amount of tracer in the Southern Ocean model domain decays exponentially, with an *e*-folding timescale of roughly 7

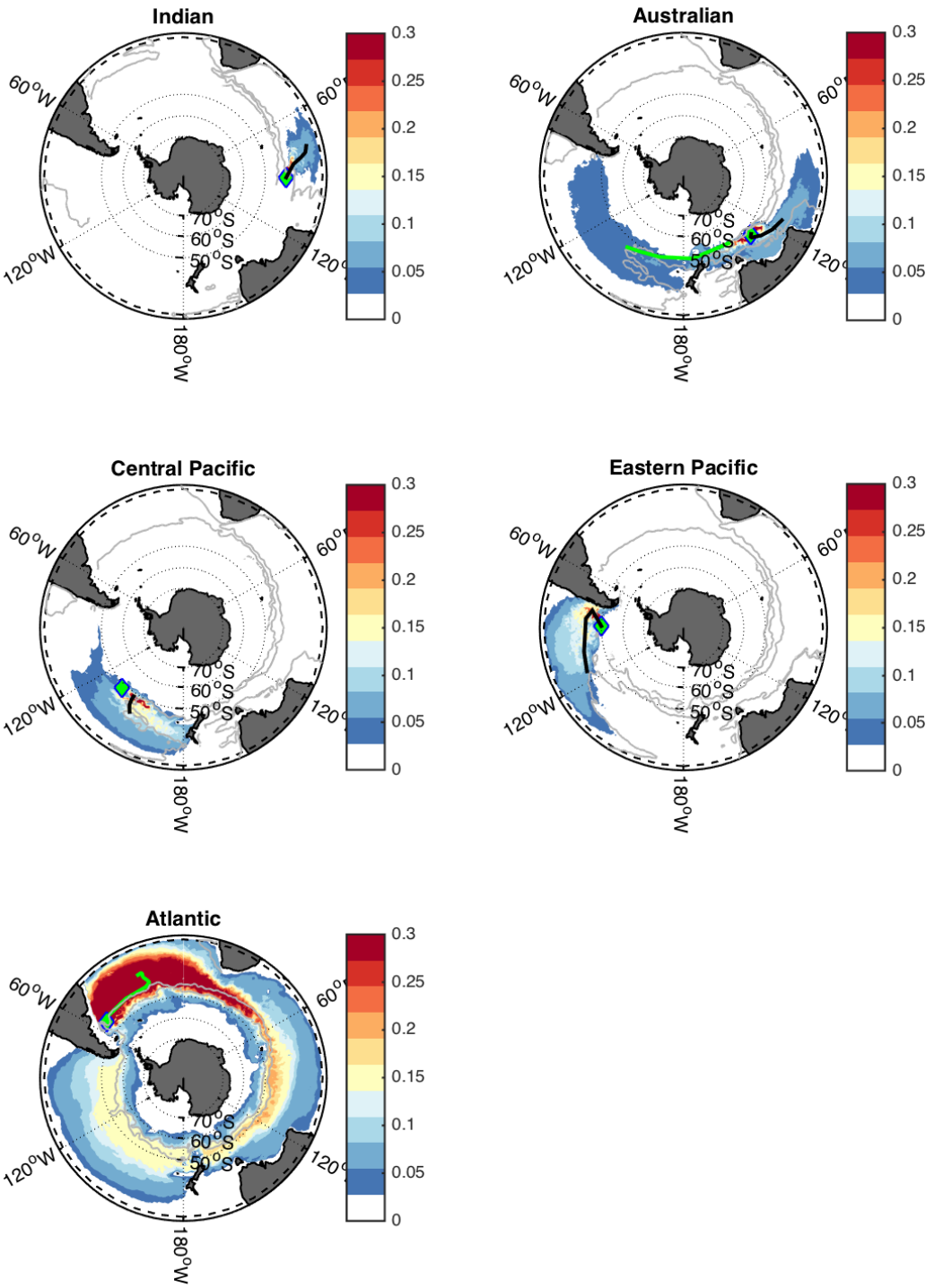

Figure 4. (a-e) Column-integrated histograms of the tracer distributions for each of the 50 year tracer advection experiments. Each color map has been scaled by the maximum concentration of each tracer, which is different for each experiment. Initial tracer locations are indicated by green diamonds. The thick solid lines show the tracer-weighted center of mass for the first 10 years of each experiment. For the Australian plot, the center of mass for just the Indian basin (i.e., Pacific basin tracer masked out) is shown in black, and the center of mass for the Pacific basin (i.e., Indian basin tracer masked out) is shown in green. The center of mass for the Atlantic tracer is shown in green for clarity on a red background. The thin gray lines are contours of the Cunningham geostrophic potential with a reference pressure of 1000 dbar on selected potential density surfaces. The black dashed line shows the location of the sponge layer.

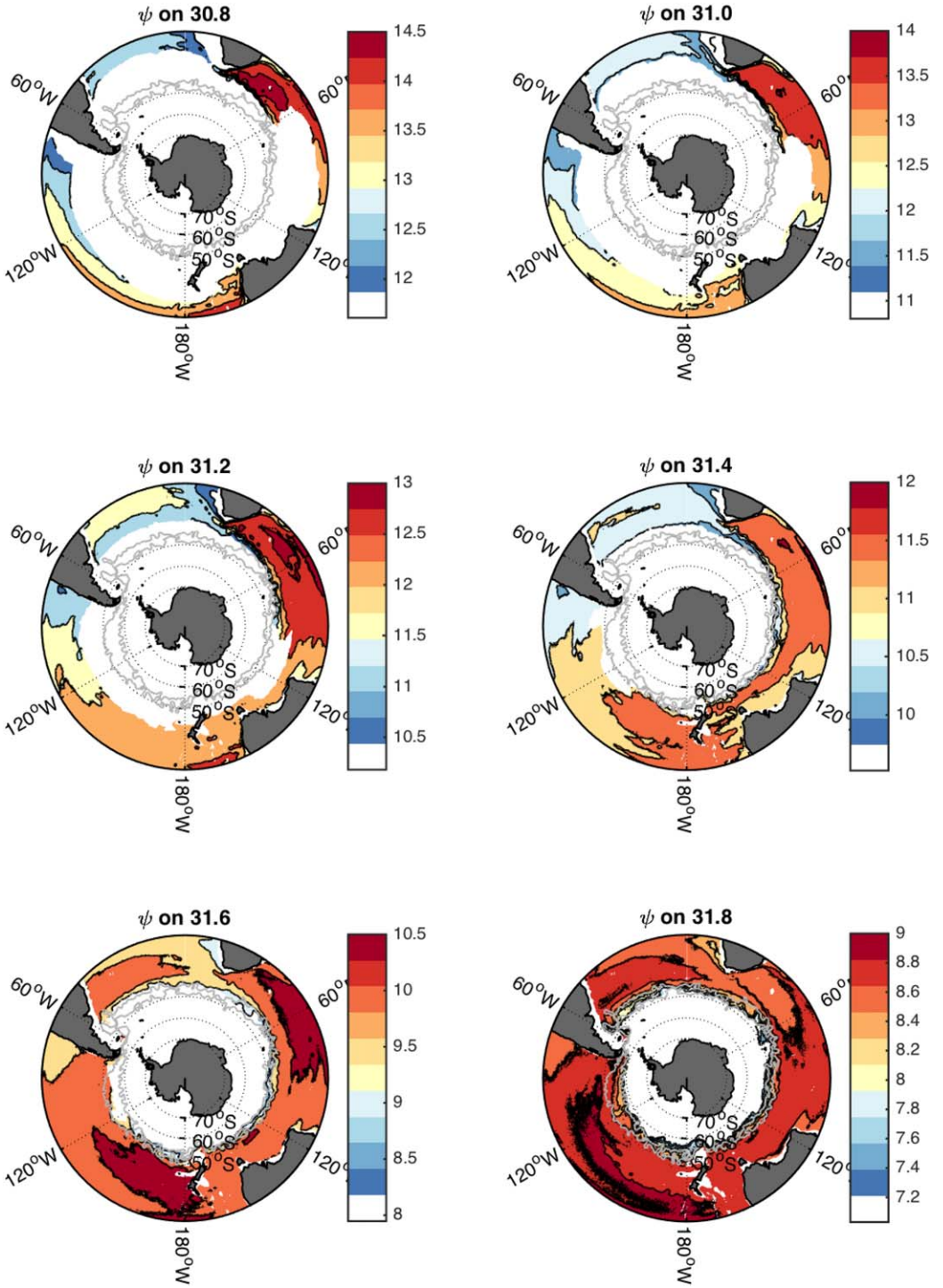

Figure 5. Cunningham geostrophic streamfunction (1 Sv = 10^6 m^3/s), derived from annual mean temperature and salinity data using the Gibbs Seawater Toolbox (GSW), with respect to 1000 dbar on several density surfaces between 30.8–31.8 kg/m^3 (*Cunningham*, 2000). The two solid lines are the 90 Sv and 130 Sv contours of the annual mean barotropic streamfunction.

years (see 6a). Once the tracer reaches South Africa, the Agulhas current (dominated by ring-like eddies) transports a small fraction of the tracer from the Indian basin to the Atlantic basin (roughly 2% of the Indian mode water tracer ends up in the Atlantic via this route). The tracer-weighted center of mass moves from (91°E, 41°S) to (70°E, 33°S) over the first 13 years of the experiment, after which the center of mass shifts southward and eastward as tracer is removed by the sponge layer.

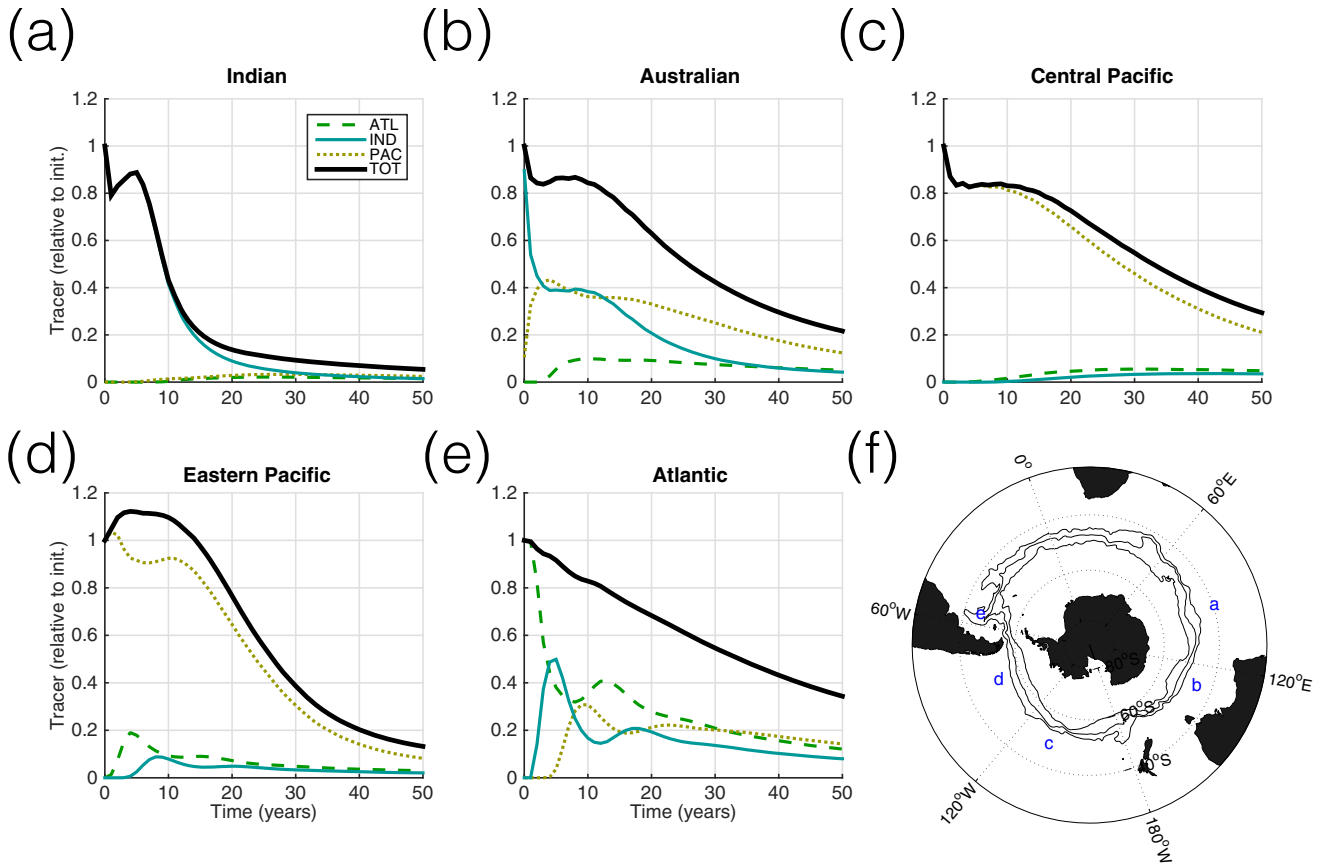

Figure 6. Time series of the total amount of tracer between 200 and 1300 m in each ocean basin, relative to the initial amount. Panels (a)-(e) correspond to tracers initialized at the five sites shown in panel (f).

3.1.2. Australian Mode Water

SAMW formed just south of Australia (i.e., initialization site initialization site "b") is heavily influenced by the ACC (Figure 4b) and is split between two basins. By year 3 of the experiment, the tracer is partitioned equally between the Indian and Pacific basins (i.e., 42% of the initial tracer in the Indian basin below 200 m, 42% of the initial tracer in the Pacific basin below 200 m, and the remaining 16% in the surface waters above 200 m). The bulk of the Australian mode water tracer is ultimately removed from the Indian basin more rapidly than from the Pacific basin, but the tracer ends up highlighting export pathways in all three basins due to the close proximity of its formation region to the ACC. The portion of the tracer that stays in the Indian basin flows westward and follows a path similar to that of the Indian SAMW. The tracer that flows eastward to the Pacific basin gradually shifts northward away from the ACC, highlighting a portion of the Pacific export pathway. Most of the tracer that flows eastward into the Pacific goes south of New Zealand and Campbell Plateau; only a small fraction flows north of New Zealand. A small fraction (less than 10%) of the tracer ends up in the Atlantic basin and exits the domain via the sponge layer there. After an initial 10 year redistribution among the basins, the total amount of tracer in the domain from the Australian pool decreases at a nearly linear rate of 19% per decade.

3.1.3. Pacific Mode Waters

The two Pacific mode water tracers (i.e. the Central Pacific and Eastern Pacific tracers, initialization sites "c" and "d" on Figure 3) both stay largely confined to the Pacific basin, although the Eastern Pacific export pathway is more rapid than the Central Pacific pathway, as indicated by the relative motion of the centers of mass and the relative tracer removal timescales. The center of mass of the Central Pacific tracer moves northward and westward toward New Zealand, from (215°E, 48°S) to (211°E, 42°S) over the first 7 years after initialization. The center of mass of the Eastern Pacific mode water tracer moves much further northward over the first 7 years after initialization, from (270°E, 50°S) to (250°E, 40°S). The eccentricities of both tracers stay between 0.96 and 1.0 from year 5 onward, indicating elliptical patterns that are stretched out in longitude by strong zonal flow. The pathways followed by both the Central Pacific and Eastern Pacific mode

water tracers are broadly consistent with the relative geostrophic flow on 31.4σ_1 and 31.6σ_1 (Figure 5). The Eastern Pacific tracer (initialization site "d") reaches the sponge layer at 26.5 °S several years earlier than the Central Pacific tracer (initialization site "c"), even though the Eastern Pacific tracer is initialized poleward of the Central Pacific tracer. From year 15 onward, the Eastern Pacific tracer is removed at a faster rate than the Central Pacific tracer (Eastern Pacific 32% per decade; Central Pacific 18% per decade). A small fraction of the Eastern Pacific tracer also ends up in the Atlantic and Indian basins much faster (peak concentration at roughly 5 years in the Atlantic and 9 years in the Indian) than the Central Pacific tracer (concentration increases slowly over 2–3 decades). The Eastern Pacific SAMW is found near a formation region of Antarctic Intermediate Water (AAIW) located off the western tip of South America, which is consistent with previous studies [e.g., *Sloyan and Rintoul* 2001, *Herraiz-Borreguero and Rintoul*, 2011]. The densest SAMW has some overlap with AAIW, so the mechanisms for AAIW export in this region are likely to also impact the export of densest SAMW.

3.1.4. Atlantic Mode Water

Finally, tracer initialized in the Atlantic mode water pool (i.e., site "e") starts in the ACC and is rapidly spread around the Atlantic, Indian, and Pacific basins. The eccentricity of the column-integrated tracer increases from 0.70 to 0.98 within the first year of the experiment due to the shearing effect of the ACC. The concentration maximum can be followed around the basins in order to estimate a rough transport timescale between them (Figure 6). The concentration of Atlantic SAMW peaks in the Indian basin roughly 5 years after tracer initialization. Peak concentration is then seen in the Pacific basin roughly 9.5 years after initialization and in the Atlantic basin roughly 13 years after initialization. There is a secondary peak in Indian basin concentration at 18 years, and a secondary peak in the Pacific after about 22 years. After 25 years, it is difficult to detect the tracer maximum as a distinct peak in the time series data. Throughout the tracer advection experiment, tracer is removed from the domain through the northern sponge layer at a rate of 15% per decade, mostly in the Atlantic basin.

3.2. Vertical Structure of Export Pathways

Each mode water tracer is initialized in a pool of low PV. The mode water pools are refreshed each winter by deep convection, which tends to mix tracer in the vertical direction. This convectively-driven vertical mixing acts in addition to down-gradient mixing brought about by the imposed background vertical diffusivity (10^{-5} m^2/s) and numerical diffusion. Thanks to this diapycnal mixing and intense surface convection, we should not expect the tracers to stay perfectly confined to density surfaces.

In Figure 7, we plot the cumulative tracer distribution over the course of the 50 year experiment in a 10° section in longitude about the time-mean center of mass of each tracer. The Indian mode water tracer mostly stays confined between 31.0 and 31.2σ_1, spreading northward and ultimately reaching the sponge layer. The influence of vertical mixing can be seen in the spread of the tracer and the fraction that reaches the surface. The Australian mode water tracer can either be followed using its Indian basin center of mass or its Pacific basin center of mass. In the Indian basin, deep convection induces diapycnal mixing, but the bulk of the tracer stays between 31.2 and 31.4σ_1. In the Pacific basin, the relative influence of the mixed layer is smaller and the diapycnal tracer spread is smaller. The Central Pacific tracer largely stays between 31.2 and 31.6σ_1, and the histogram is dominated by the bulk of tracer that slowly moves away from the initialization site. The Eastern Pacific tracer histogram is spread much further northward, as the Eastern Pacific export pathway is more rapid than the Central Pacific pathway.

In Figure 8, we plot the vertical partitioning of tracers with depth over the course of the 50 year experiment. In each of the experiments, a fraction of each tracer (less than 20–30% of the initial amount) ends up in the upper 200 m due to interactions with the mode water tracers and the mixed layer. The fraction of the initial tracer located below 500 m increases over the first 10 years as the tracers are subducted, guided by isopycnals that slope downward toward the equator. The fraction of tracer below 500 m could be considered reasonably well "subducted" below the mixed layer, and the fraction below 1000 m is completely subducted. The fraction of total tracer below 1000 m increases in each experiment (Figure 8f). The subducted tracer will ventilate the deep thermocline via export hotspots.

3.3. Mode Water Decay

As SAMW advects, it mixes with the surrounding water masses and thereby gradually loses its characteristic density range and anomalously low potential vorticity. In order to quantify the timescales over which

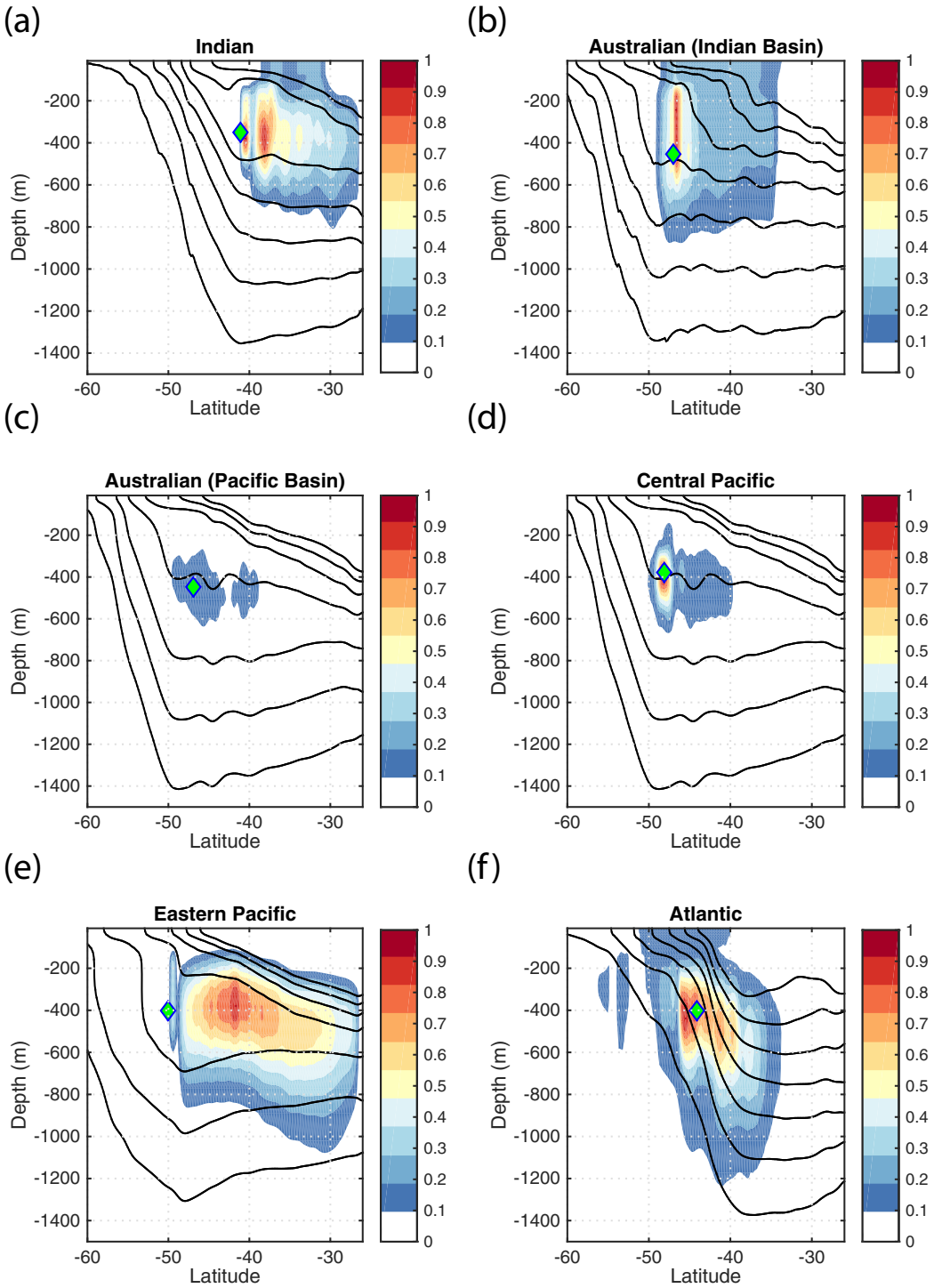

Figure 7. Tracer distribution histograms for each of the 50 year tracer advection experiments. Each color map has been scaled by the maximum concentration of each tracer, which is different for each experiment. Initial locations are indicated by green diamonds. The black solid lines are σ_1 potential density surfaces (30.8–32.0 kgm^{-3}, every 0.2 kgm^{-3}). The tracer concentrations and potential densities are averaged in 10° wide swaths about the longitudes of the tracer centers of mass. (b) Only includes Australian tracer located in the Indian basin, and (c) only includes Australian tracer located in the Pacific basin.

SAMW changes density class, we calculate the fraction of tracer that is lighter than SAMW ($<31.0\sigma_1$), in the SAMW density range (31.0–31.8σ_1), or denser than SAMW ($>31.8\sigma_1$) (Figure 9). Over the first decade of each experiment, we find average SAMW density decay rates between 2–5%/yr relative to the initial tracer in each experiment (Indian - 5.0%/yr; Australian - 2.0%/yr; Central Pacific - 1.6%/yr; Eastern Pacific - 1.4%/yr;

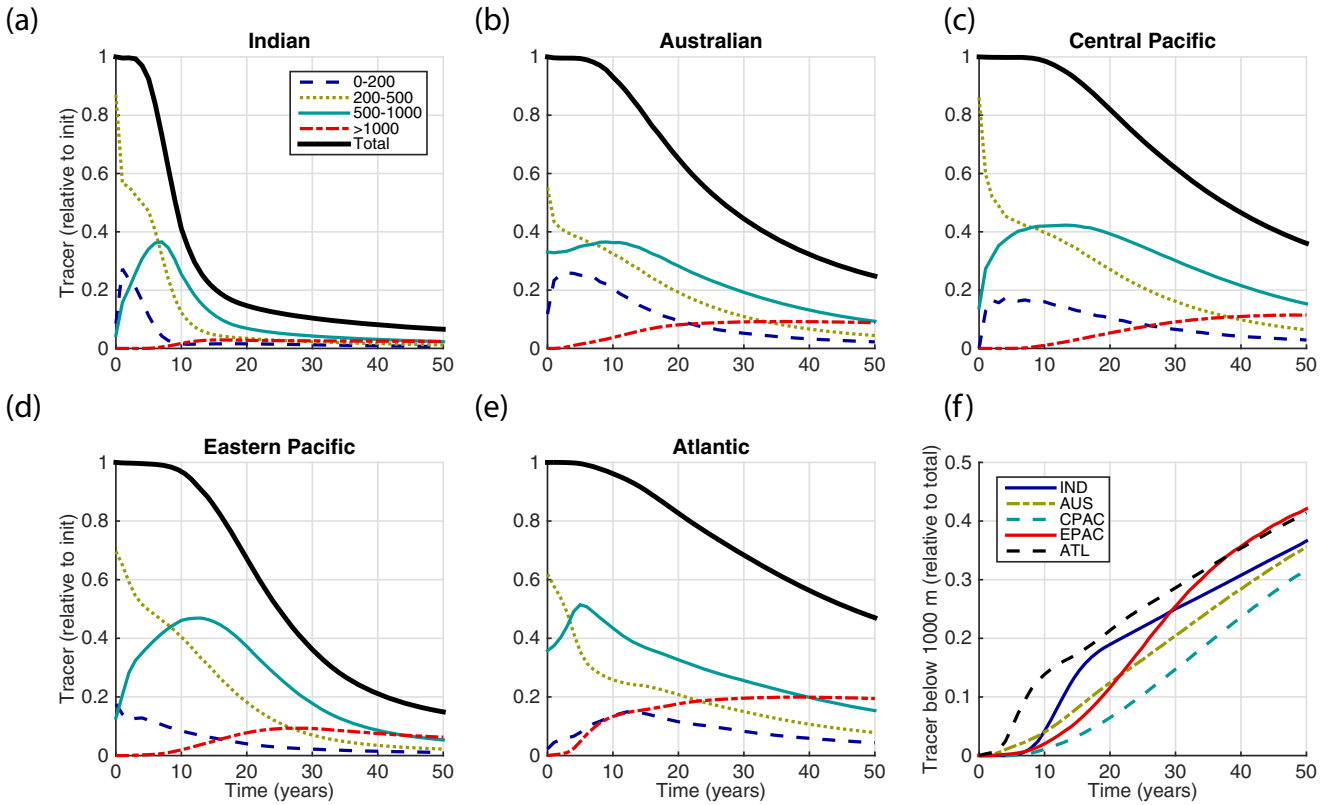

Figure 8. (a-e) Time series of the vertical distribution of tracer, relative to the initial amount of tracer used in each experiment. The initial tracer locations are shown in Figure 6f. (f) The fraction of the remaining tracer that is found below 1000 m over the course of each experiment.

and Atlantic - 3.5%/yr). During this time period, mode water loss in the Indian and Central Pacific is largely due to transformation into lighter density classes, whereas mode water loss in the Atlantic is nearly all due to transformation into denser classes. Australian losses are dominated by transformation into lighter classes, and in the Eastern Pacific loss is roughly equal parts transformation into lighter and denser classes.

After 10 years of advection, sponge layer removal contributes to SAMW loss in all five tracer experiments. One way to adjust for this effect is to scale the amount of tracer in a density class by the total amount of tracer found in the model domain (Figure 9f). In order to estimate SAMW decay timescales, we fit two-term exponential models to each SAMW time series ($R^2 > 0.9$ in all five cases), where each time series has been scaled by the remaining tracer in each experiment. We find *e*-folding SAMW decay timescales between 50–20 years (Indian—76 years; Australian—84 years; Central Pacific—118 years; Eastern Pacific—50 years; Atlantic—69 years). These multidecadal timescales are broadly consistent with other estimates of SAMW lifetime [e.g., *Primeau and Holzer*, 2006; *Trossman et al*., 2012]. Note that nearly all of these timescales are longer than the duration of our simulation; this analysis assumes that decay rates will continue to be well-represented by a double exponential model well beyond the 50 year simulation.

3.4. Export Hotspots

Once tracer hits the northern boundary of the model domain (24.7–26.5 °S), it is removed by a sponge layer (i.e., the tracer field is relaxed to zero with a timescale of about 6 h). We use this removal as a proxy for thermocline ventilation. In this section, we examine the longitudes, depths, and timescales on which the mode water tracers are removed in order to discuss how mode water origin water parcels ultimately cross 26.5 °S. These results must be interpreted in the context of our choice of model domain, i.e., the timescales and removal will be different with a different choice of northern boundary. In Figure 10, we plot timeseries of the cumulative amount of tracer that is removed by the sponge layer in the upper ocean (i.e., above the 200 m depth, where 200 m is chosen as it is well below the shallow subtropical mixed layer), the cumulative

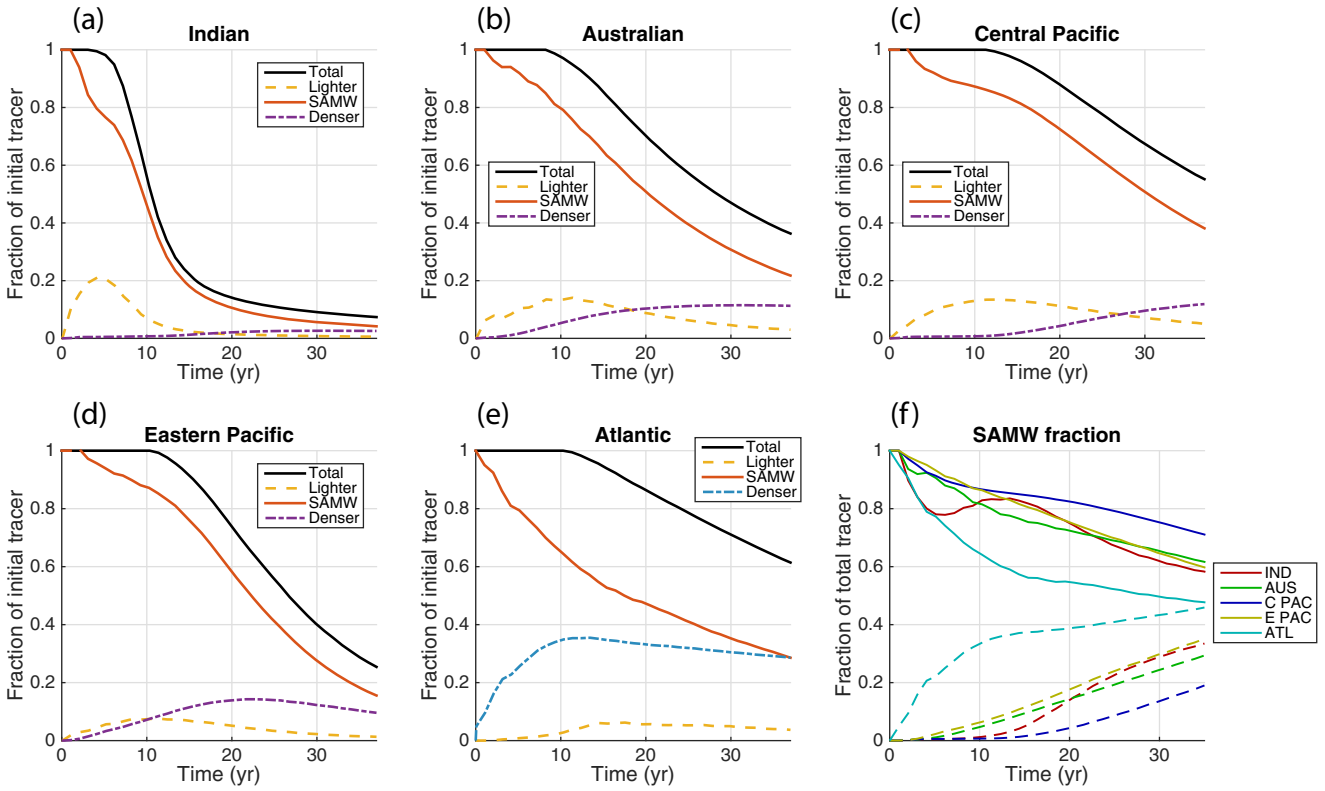

Figure 9. (a-e) Time series of the proportion of each mode water tracer that is less dense than SAMW ("lighter," $<31.0\sigma_1$), in the SAMW density range ($31.0–31.8\sigma_1$), or more dense than SAMW ($>31.8\sigma_1$), relative to the initial amount of tracer used in each experiment. The initial tracer locations are shown in Figure 6f. (f) The SAMW fraction of each mode water tracer (solid lines) and the fraction denser than SAMW (dashed lines), relative to the total amount of remaining tracer in the model domain.

amount removed by the sponge layer in the interior ocean (i.e., below 200 m), and the total tracer in the Southern Ocean domain.

Over the course of a 50 year tracer transport experiment, we find that less than 15% of each mode water tracer crosses 26.5 °S above 200 m, which is one measure of the efficiency with which the mode water pools ventilate the subtropical thermocline (i.e., a small percentage implies efficient subduction). The Eastern Pacific pathway is especially efficient, with less than 10% removed from or remaining in the upper 200 m by year 50. The time required for 50% of a chosen mode water tracer to be removed from the Southern Ocean domain varies greatly across initialization sites (i.e., 9 years Indian, 27 years Australian, 37 years Central Pacific, 25 years Eastern Pacific, 47 years Atlantic), reflecting the different latitudes of the initialization sites, the relative importance of circumpolar (i.e., ACC) and gyre-like circulation, and regional circulation variability.

In Figure 11, we plot the cumulative removal of tracer by the sponge layer over the course of the 50 year experiment. The bulk of the tracers are removed at depths below their initialization depths, which is consistent with geostrophic flow guided by isopcynals that slope downward toward the equator. Also, the bulk of the tracers are removed to the west of the tracer initialization sites, which is consistent with large-scale subtropical gyre circulation in these regions. One exception is the Atlantic tracer, which is dominated by the circumpolar flow of the ACC. The Atlantic tracer is largely removed in the boundary current east of South America, but most of it has not yet been removed by the end of the experiment. The contrasting removal patterns of the two Pacific basin tracers reflect strong regional differences in their export pathways. The Central Pacific tracer follows a slow gyre circulation and has time to spread westward before interacting with the sponge layer. By contrast, the Eastern Pacific tracer rapidly moves up the coast of South America during the first decade of its advection, so it does not have time to spread as far west before removal. Nevertheless, there is some overlap between the Central Pacific and Eastern Pacific removal patterns, indicating that the two pathways are not totally distinct.

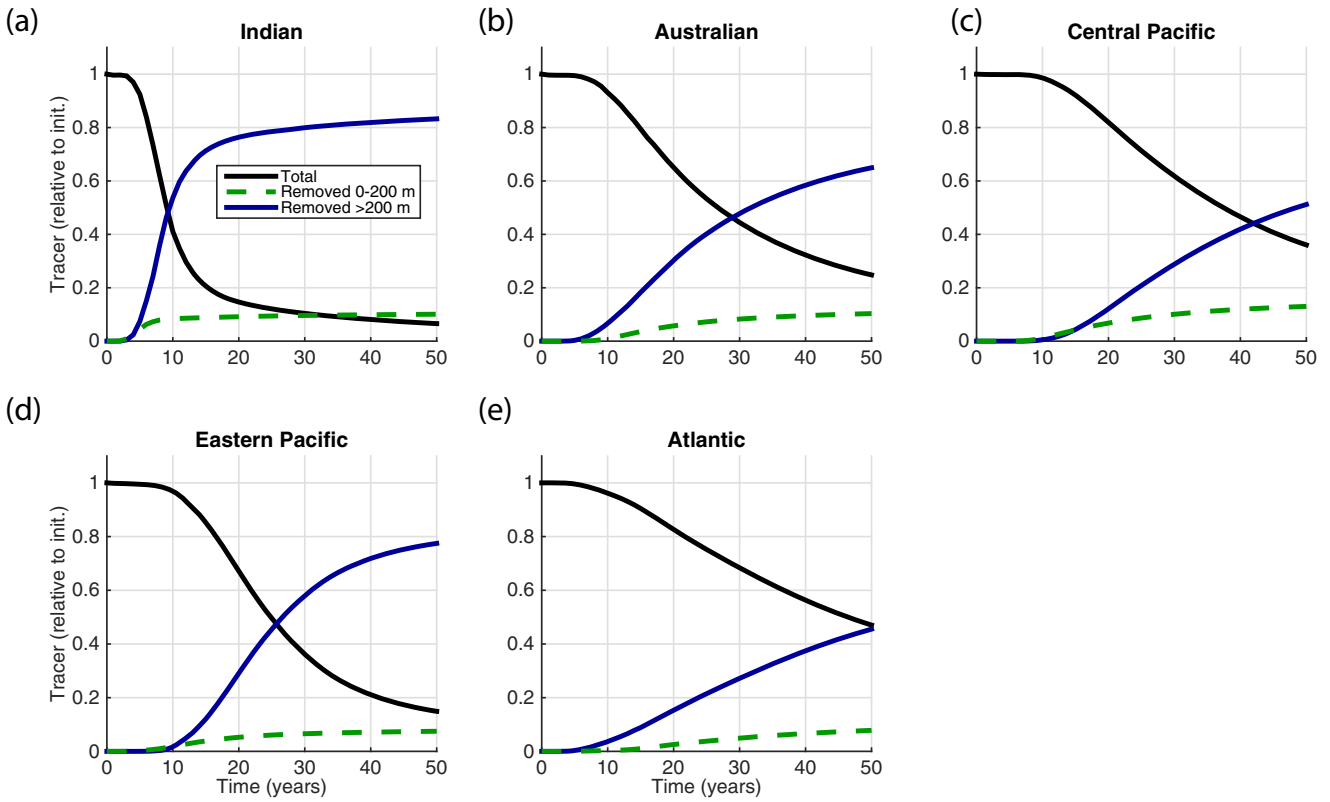

Figure 10. Total amount of tracer in the Southern Ocean domain for each experiment (black solid lines), fraction of tracer removed above 200 m (green dashed lines), and the fraction of tracer removed below 200 m (blue solid lines).

3.4.1. Analysis

In this section, we examine tracer-weighted quantities for signatures of mixing and advection. All of the tracer-weighted centers of mass (COM) get deeper over the first 10 years of the experiment (Figure 12a). The COM generally progress northward, with the exception of the Atlantic tracer, which over the first decade stays roughly constant (within 2 degrees latitude) as much of the tracer is advected around the ACC Figure 12b). There is no "error" (Δf) in latitude because the tracer-weighted latitudes are effectively frozen at 26.5 °S as tracer exits the Southern Ocean domain.

The Indian tracer gets warmer and saltier as it moves northward, becoming less dense overall through diapycnal fluxes. The Australian tracer gets denser by roughly 0.1 kg/m^3 as it cools and freshens, mixing with the Indian Deep Water (IDW). The regional contrast between the Indian and Australian tracers indicates that the Indian pool is closer than the Australian pool to the "upwelling" region (i.e., where SAMW mixes back up to the surface). However, more than 80% of the Indian tracer is removed below 200 m, which is a high percentage relative to the other tracers. The Indian tracer is possibly more likely to upwell faster than the Australian tracer once it crosses north of 26.5 °S, but it is still a relatively efficient pathway for the initial export into the subtropical thermocline.

Both the Central Pacific and the Eastern Pacific centers of mass stay roughly constant in density (within 0.02 kg/m^3), indicating that they are relatively well-insulated from the mixed layer and in a region where diapycnal mixing is weak or isotropic. The Central Pacific patch gets cooler and fresher, while the Eastern Pacific patch gets warmer and saltier. The regional contrast between the Central and Eastern Pacific is consistent with the Eastern Pacific tracer's relatively more rapid progression to lower latitudes, where it can mix with lighter waters. The Atlantic tracer density stays within 0.02 kg/m^3 of its starting value over the first decade of the simulation; it gets considerably warmer and saltier as it mixes with the Algulhas waters off the coast of South Africa.

4. Discussion

In this work, we performed numerical tracer initialization experiments to map out the export pathways of Subantarctic Mode Water (SAMW) and to better understand the associated ventilation of the subtropical

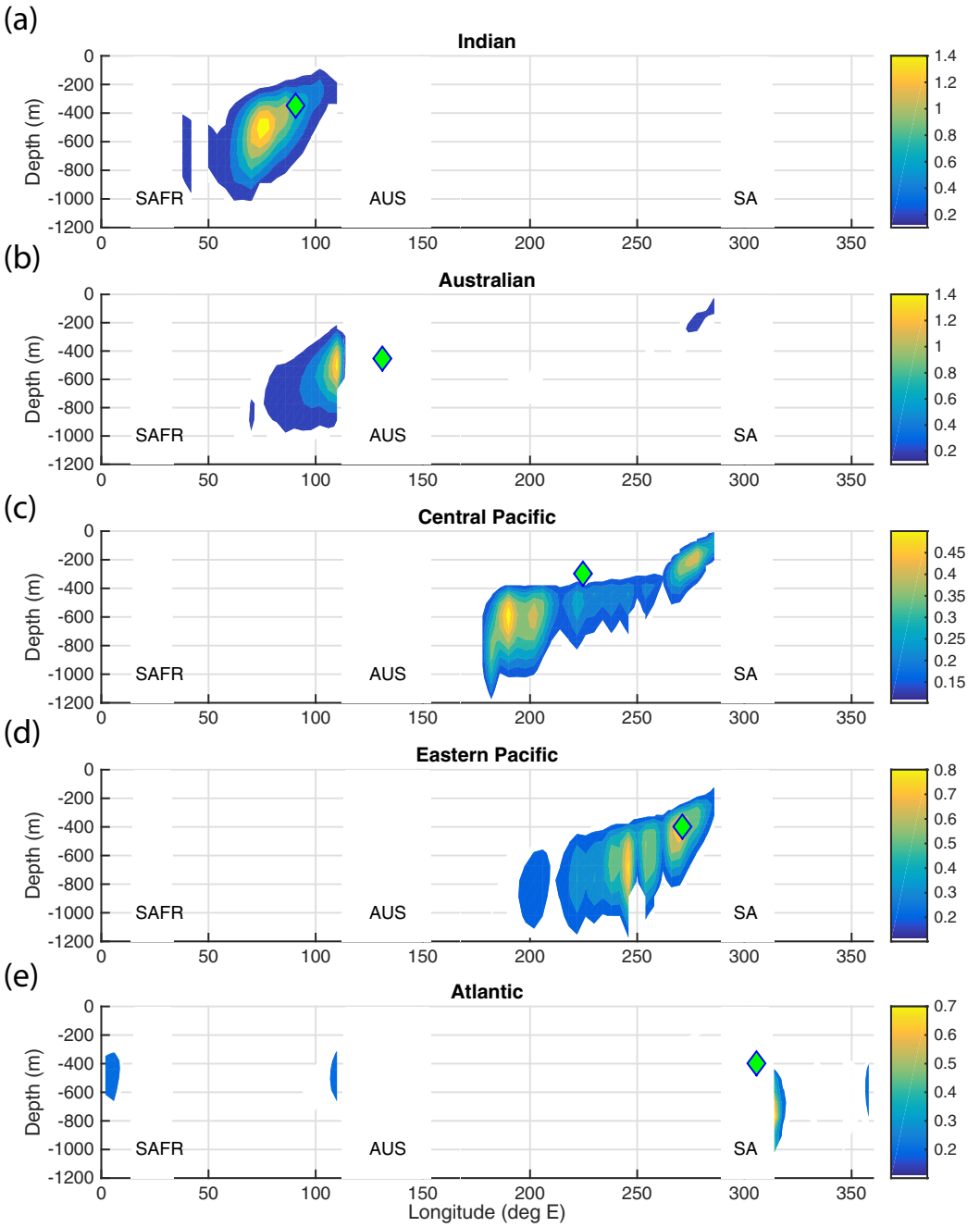

Figure 11. Spatial distribution of the cumulative tracer removed by the sponge at the northern boundary (24.7–26.5 °S) 50 years into the experiment, as a fraction of the initial tracer. Shown from top to bottom are the (a) Indian, (b) Australian, (c) Central Pacific, (d) Eastern Pacific, and (e) Atlantic tracer advection experiments. Approximate initial tracer locations are indicated by green diamonds. Removal percentages have been summed onto a grid with 90 points in the horizontal and 42 points in the vertical for clarity.

thermocline. We found considerable regional variability in the patterns, timescales, and efficiencies of SAMW export, set in part by the relative influence of the Antarctic Circumpolar Current (ACC) and the subtropical gyres. The spatial structure of the export pathways is broadly consistent with the mean geostrophic circulation, which in the gyres is constrained by basin-scale pressure gradients [*Iudicone et al.*, 2007]. Export from the Indian and Central Pacific mode water pools are primarily driven by large-scale gyre circulation, whereas the Australian and Atlantic pools are heavily influenced by the Antarctic Circumpolar Current. Export from the Eastern Pacific mode water pool is driven by a combination of a deep eastern boundary current and subtropical gyre circulation. The tracer distributions and removal maps presented in this paper

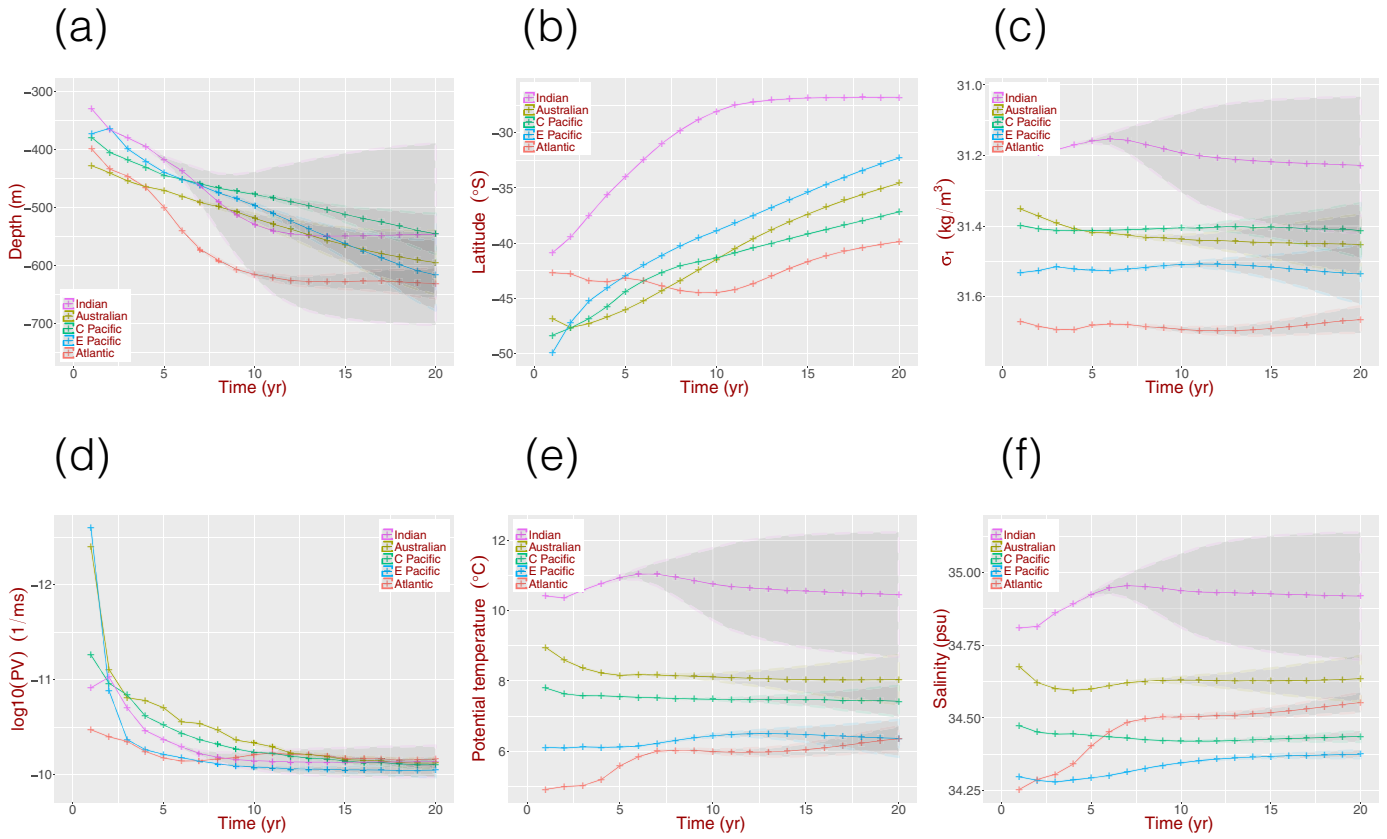

Figure 12. Tracer-weighted mean quantities for the five tracer advection experiments. Shown are (a) depth, (b) latitude, (c) potential density, (d) potential vorticity, (e) potential temperature, and (f) salinity. Shading indicates the uncertainty introduced by removal via the sponge layer at the northern edge of the domain. Tracer above 200 m is masked out, so these values reflect ocean interior properties.

(i.e., Figures 4 and 11) indicate the broad regions where we expect northward export, neglecting recirculation/re-entrance, to occur.

Export of the Indian mode water tracer (i.e., initialization site "a" in Figure 3) is dominated by the subtropical Indian Ocean Gyre; it is minimally affected by the strong zonal circulation of the ACC. In the global ocean, this exported SAMW upwells together with the denser Indian Deep Water (IDW) and joins with thermocline water coming through the Indonesian Throughflow before returning to the ACC [*Talley*, 2013, references therein]. We find relatively little mode water tracer in the Pacific and Indian basins after 50 years, as most of it has been removed by the sponge layer. In the global ocean, the Indian mode water that eventually is found in the other basins may first be carried through the return flow of the shallow Indian basin overturning circulation.

The Australian mode water tracer (i.e., initialization site "b" in Figure 3) is heavily affected by the ACC. The tracer is split into two separate patches that advect into both the Indian and Pacific basins. The bulk of this tracer crosses 30°S just east of Australia, following the subsurface West Australian Current. The remaining tracer stays largely confined to the ACC and does not exit the model domain over the 50 year experiment. Considering the Indian and Australian mode water tracers together, we suggest that the "youngest" mode water (i.e., the mode water with the most recent contact with the atmosphere and surface mixed layer) exported from the Indian basin into the Pacific primarily comes from the Australian pool (i.e., initialization site "b") and not from the Indian pool (i.e., initialization site "a").

The two Pacific basin export pathways highlighted by the tracers have remarkably different structures. The Central Pacific mode water tracer (i.e., initialization site "c" in Figure 3) is removed relatively slowly from the basin by the action of the South Pacific gyre. The bulk of this tracer (i.e., more than 90%) remains in the Pacific basin and is removed east of its formation region. In the global ocean, this SAMW mixes with upwelling PDW in the subtropics to become thermocline water [*Talley*, 2013]. The thermocline water formed

Table 3. Summary of Tracer Advection Results

Basin	Initial Latitude (S)	Removal Timescale (Years)	Remaining in Basin (10 Years)	Removed Above 200 m (50 Years)	Removed Below 200 m (50 Years)
Indian	41	9	41%	10%	83%
Australian	47	27	38%	10%	65%
C. Pacific	48	37	81%	13%	51%
E. Pacific	50	25	92%	7%	77%
Atlantic	44	47	35%	8%	46%

[a]All tracer fractions are given as percentages of the initial amount of tracer in each experiment. The removal timescale is the time required for at least 50% of the initial tracer to be removed from the model domain. The column labeled "remaining in basin" refers to the basin in which the tracer was initialized, 10 years into the experiment. The sum of the last two columns gives the total amount removed by the sponge layer at the northern edge of the domain, 50 years into the experiment.

in the Central Pacific makes its way through the Indonesian Throughflow and joins the poleward flow in the Indian basin.

The Eastern Pacific mode water tracer (i.e., initialization site "d" in Figure 3) quickly advects equatorward, following the southern part of the Humboldt Current System along the west coast of South America, before joining the subtropical gyre. The export route of this Eastern Pacific mode water is closely related to (and has some overlap with) the AAIW export pathway discussed in *Iudicone et al*. [2007]. Approximately 5 years into the experiment, roughy 20% of the initial Eastern Pacific mode water tracer has been advected through the ACC and is found in the Atlantic basin, which suggests that a fraction of mode water formed in the Eastern Pacific can make its way to the Atlantic mode water pool (i.e., initialization site "d" in Figure 3). The Atlantic mode water tracer stays largely confined to the ACC over the course of the experiment; it is largely "trapped" in the circumpolar flow and highlights a relatively inefficient pathway for getting mode waters out of the Southern Ocean.

One relatively simple metric of SAMW "export efficiency" consists of how much mode water tracer (i.e., tracer initialized in the mode water formation regions) remains in a chosen domain as a function of time. In our numerical experiments, more than 50% of each mode water tracer reaches the subtropical thermocline (defined as absorption by the sponge layer between 24.7 and 26.5 °S) within 50 years. The Eastern Pacific pathway is an especially efficient mode water export route, with roughly 80% entering the subtropical thermocline within 50 years. The time required for 50% of the mode water tracers to leave the Southern Ocean domain varies significantly between mode water pools, from 9 years for the Indian mode water pool to roughly 38 years for the Central Pacific mode water pool. The removal timescales and distributions are summarized in Table 3.

4.1. Future Changes in SAWM

SAMW and AAIW are relatively sensitive indicators of anthropogenic climate change in coupled climate models [*Banks et al*., 2000, 2002; *Banks and Bindoff*, 2003; *Stark et al*., 2006]. Understanding the timescales and spatial patterns of thermocline ventilation via SAMW and AAIW will help us understand how surface ocean signals of climate change may ultimately propagate into the subtropical thermocline. For instance, repeat hydrography sections indicate that in the 2000s, Southern Hemisphere thermocline oxygen increased due to stronger wind forcing and ventilation [*Talley et al*., 2016]. Many coarse resolution models project a decrease in the subduction of SAMW and AAIW under climate change, due to increased surface warming and freshening [*Downes et al*., 2010]. Given that the subtropical portions of the export pathways are relatively well insulated from the surface, their response to anthropogenic forcing will lag far behind that of SAMW and AAIW subduction. If equatorward export rates and pathways remain relatively steady under climate change, then decreased SAMW/AAIW subduction suggested by *Downes et al*. [2010] will result in a thinning of those water masses in subtropical latitudes and an associated decrease in nutrient export and anthropogenic carbon sequestration in the subtropical thermocline. More detailed studies with representations of the marine nutrient and carbon cycles are required to better understand how nutrient export and carbon sequestration may be impacted by anthropogenic forcing. Furthermore, the "transition region dynamics" between the ACC and the subtropical gyres that allow some fraction of mode waters to separate from the ACC and join the gyres remains poorly understood. A particular area of interest is how these mechanisms contrast with inter-gyre exchange processes in the Northern Hemisphere [*Pedlosky*, 1984; *Schopp and Arhan*, 1986; *Chen and Dewar*, 1993; *Iudicone et al*., 2007].

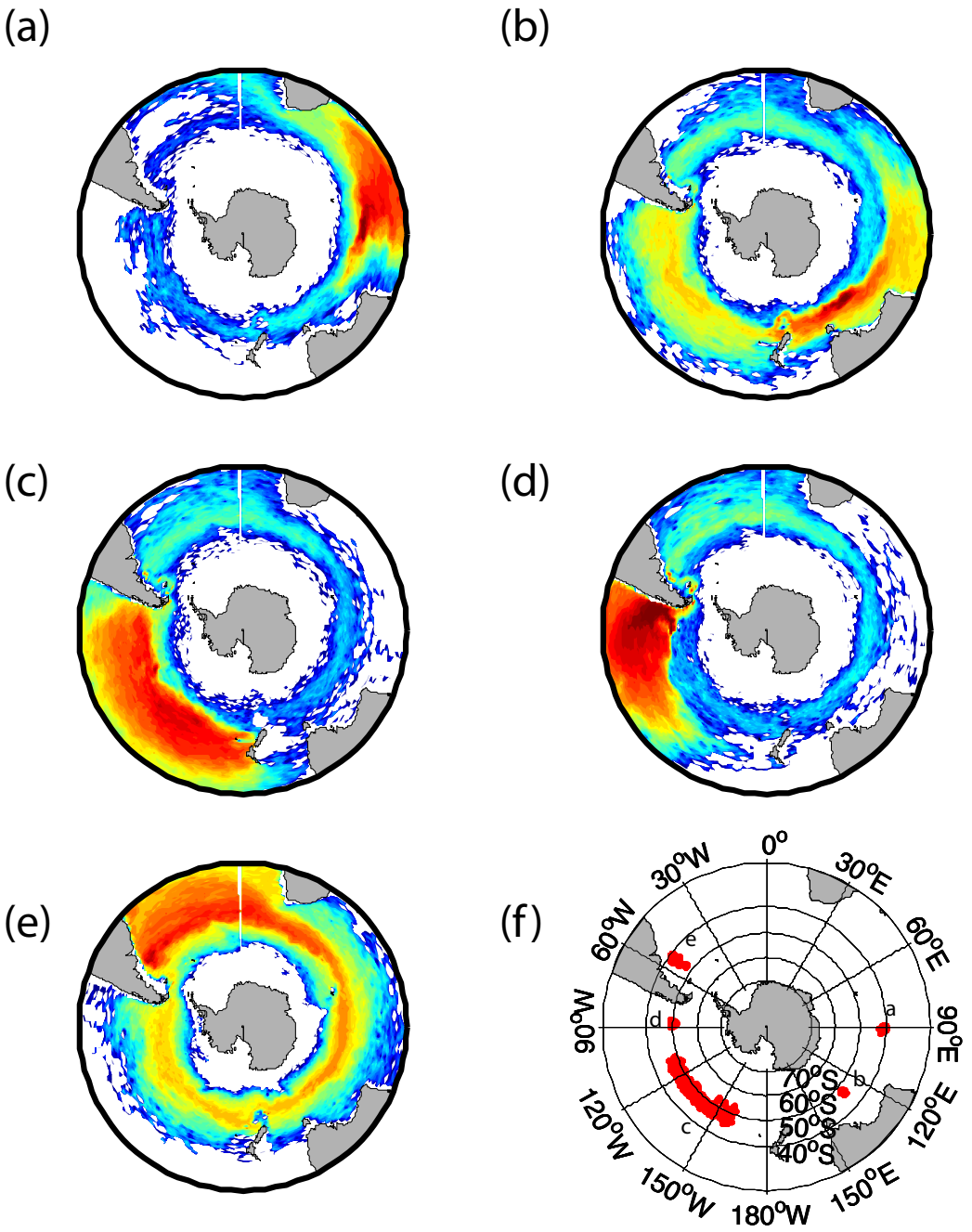

Figure 13. (a-e) Particle trajectories traced out after 10 years of advection. (f) Particle initial locations of experiments shown in Figures 13a–13e.

4.2. Effects of Unresolved Eddies

Turbulent mixing along isopycnals likely influences SAMW advection and erosion [*Musgrave*, 1990; *Trossman et al*., 2012; *Abernathey and Ferreira*, 2015]. BASSOON is an eddy-permitting model; in the open ocean north of the ACC, where most of our tracer advection occurs, larger mesoscale features are fully resolved and do not suffer from artificial smoothing from over-parameterization [*Hallberg*, 2013]. However, because BASSOON does not use any subgrid scale parameterization schemes (except for vertical mixing by KPP), it neglects sub-mesoscale effects and the smallest mesoscale features. In shallow, near-coastal shelves and plateaus, where the baroclinic deformation radius is not resolved, eddy mixing may be biased toward weak values, which may impact export timescales and pathways. In our numerical experiments, this bias is

particularly relevant for (i.) the portion of Indian Mode Water tracer that advects into the Atlantic basin via the Agulhas current, (ii.) the portion of Australian and Central Pacific tracers that advect over Campbell Plateau and generally around New Zealand, and (iii.) the portion of the Atlantic tracer that advects over the Patagonian Shelf. It would be instructive to perform SAWM tracer release experiments using modeling environments with various mesoscale and sub-mesoscale eddy parameterization schemes [e.g., *Fox-Kemper et al*., 2011; *Jansen and Held*, 2014] and observationally informed data products [e.g., *Abernathey and Marshall*, 2013; *Waterhouse et al*., 2014; *Whalen et al*., 2015].

4.3. Comparison With Numerical Float Advection

In order to illustrate the robustness of the broad structure of the export pathways (i.e., to show that they are not tracer artifacts), we also advected floats (using the MITgcm "flt" package) using an offline 20 year velocity data set extracted with 5 day averages from an online run of BASSOON. We plot the cumulative trajectory histogram in Figure 13. The float patterns are broadly similar to those followed by the tracers (Figure 4) and outlined by the mean flow (Figure 5). The Indian basin floats mostly stay confined to the Indian basin, although some do reach the Agulhas Current and advect into the Atlantic basin. The Australian floats are heavily influenced by the ACC And spread across all three basins. The Central Pacific floats largely follow the gyre, while the Eastern Pacific floats quickly move up the coast of South America before spreading out westward via the subtropical gyre. The Atlantic floats largely stay in the ACC, ending up in all three basins.

5. Conclusions

Subantarctic Mode Water (SAMW) is an important mode water class for subtropical thermocline ventilation, which impacts anthropogenic carbon sequestration and the export of nutrients to lower latitudes. The export of mode water displays significant regional variability, heavily influenced by the regional structures of the mean geostrophic circulation. More than 50% of each mode water tracer reaches the subtropical thermocline within 50 years, but the Eastern Pacific pathway is especially efficient, with roughly 80% entering the subtropical thermocline within 50 years. The time required for 50% of the mode water tracers to leave the Southern Ocean domain varies significantly between mode water pools (see Table 3 for a summary). Export from the Indian and Central Pacific mode water pools is primarily driven by large-scale gyre circulation, whereas the Australian and Atlantic pools are heavily influenced by the Antarctic Circumpolar Current. Export from the Eastern Pacific mode water pool is driven by a combination of deep boundary currents and subtropical gyre circulation. Additional work focusing on anthropogenic carbon sequestration and nutrient export would be a welcome addition to this study.

Acknowledgments

This work was supported by the Natural Environment Research Council (NERC grant NE/J007757/1) and used the ARCHER UK National Supercomputing Service (http://www.archer.ac.uk). Matt Mazloff acknowledges the National Science Foundation (NSF) for support of this research through grants OCE-1234473 and PLR-1425989. The authors thank Lynne *Talley*, Jinbo Wang, and an anonymous reviewer for comments that greatly improved the quality of this paper. The model used (MITgcm) is available at http://mitgcm.org/, and other data are available on the SOSE website (http://sose.ucsd.edu/) and in the references of this paper.

References

Abernathey, R., and D. Ferreira (2015), Southern Ocean isopycnal mixing and ventilation changes driven by winds, *Geophys. Res. Lett.*, *42*, 10,357–10,365, doi:10.1002/2015GL066238.

Abernathey, R., and J. Marshall (2013), Global surface eddy diffusivities derived from satellite altimetry, *J. Geophys. Res. Oceans*, *118*, 901–916, doi:10.1002/jgrc.20066.

Banks, H., and N. Bindoff (2003), Comparison of observed temperature and salinity changes in the Indo-Pacific with results from the coupled climate model HadCM3: Processes and mechanisms, *J. Clim.*, *16*, 156–166.

Banks, H., R. Wood, J. Gregory, T. C. Johns, and G. S. Jones (2000), Are observed decadal changes in intermediate water masses a signature of anthropogenic climate change?, *Geophys. Res. Lett.*, *27*(18), 2961–2964, doi:10.1029/2000GL011601.

Banks, H., R. Wood, and J. Gregory (2002), Changes to Indian Ocean subantarctic mode water in a coupled climate model as CO_2 forcing increases, *J. Phys. Oceanogr.*, *32*, 2816–2827.

Cerovečki, I., and M. Mazloff (2015), The spatiotemporal structure of diabatic processes governing the evolution of subantarctic mode water in the Southern Ocean, *J. Phys. Oceanogr.*, *46*, 683–710, doi:10.1175/JPO-D-14-0243.1.

Cerovečki, I., L. Talley, M. Mazloff, and G. Maze (2013), Subantarctic mode water formation, destruction, and export in the eddy-permitting Southern Ocean state estimate, *J. Phys. Oceanogr.*, *43*(7), 1485–1511, doi:10.1175/JPO-D-12-0121.1.

Chelton, D., R. DeSzoeke, M. Schlax, K. E. Naggar, and N. Siwertz (1998), Geographical variability of the first baroclinic Rossby radius of deformation, *J. Phys. Oceanogr.*, *28*, 433–460.

Chen, L., and W. Dewar (1993), Intergyre communication in a three-layer model, *J. Phys. Oceanogr.*, *23*, 855–878.

Comiso, J. (2015), *Bootstrap Sea Ice Concentrations From Nimbus-7 SMMR and DMSP SSM/I-SSMIS, Version 2*, NASA Natl. Snow and Ice Data Cent. Distrib. Active Arch. Cent., Boulder, Colo., doi:10.5067/J6JQLS9EJ5HU.

Cunningham, S. A. (2000), Circulation and volume flux of the North Atlantic using synoptic hydrographic data in a Bernoulli inverse, *J. Marine Res.*, *58*, 1–35.

Downes, S., N. Bindoff, and S. Rintoul (2010), Changes in the subduction of Southern Ocean water masses at the end of the twenty-first century in eight IPCC models, *J Clim.*, *23*, 6526–6541, doi:10.1175/2010JCLI3620.1.

Downes, S. M., A. S. Budnick, J. L. Sarmiento, and R. Farneti (2011), Impacts of wind stress on the Antarctic Circumpolar Current fronts and associated subduction, *Geophys. Res. Lett.*, *38*, L11605, doi:10.1029/2011GL047668.

Fox-Kemper, B., G. Danabasoglu, R. Ferrari, S. Griffies, R. Hallberg, M. Holland, M. Maltrud, S. Peacock, and B. Samuels (2011), Parameterization of mixed layer eddies. iii: Implementation and impact in global ocean climate simulations, *Ocean Modell.*, *39*(1–2), 61–78, doi:10.1016/j.ocemod.2010.09.002.

Hallberg, R. (2013), Using a resolution function to regulate parameterizations of oceanic mesoscale eddy effects, *Ocean Modell.*, *72(C)*, 92–103, doi:10.1016/j.ocemod.2013.08.007.

Hanawa, K., and L. Talley (2001), *Mode Waters. Ocean Circulation and Climate*, *Int. Geophys. Ser*, edited by G. Siedler and J. Church, pp. 373-386, Academic Press.

Herraiz-Borreguero, L., and S. Rintoul (2011), Subantarctic mode water: Distribution and circulation, *Ocean Dyn.*, *61*(1), 103–126.

Heuzé, C., K. J. Heywood, D. P. Stevens, and J. K. Ridley (2013), Southern Ocean bottom water characteristics in CMIP5 models, *Geophys. Res. Lett.*, *40*, 1409–1414, doi:10.1002/grl.50287.

Holland, P. R., N. Bruneau, C. Enright, M. Losch, N. T. Kurtz, and R. Kwok (2014), Modeled trends in Antarctic sea ice thickness, *J Clim.*, *27*(10), 3784–3801, doi:10.1175/JCLI-D-13-00301.1.

Ito, T., M. Woloszyn, and M. Mazloff (2010), Anthropogenic carbon dioxide transport in the Southern Ocean driven by Ekman flow, *Nature*, *463*, 80, doi:10.1038/nature08687.

Iudicone, D. (2010), Watermasses as a unifying framework for understanding the Southern Ocean carbon cycle, *Biogeosci. Discuss.*, *7*, 3392–3451, doi:10.5194/bgd-7-3393-2010.

Iudicone, D., K. Rodgers, R. Schopp, and G. Madec (2007), An exchange window for the injection of antarctic intermediate water into the south pacific, *J. Phys. Oceanogr.*, *37*, 31–49, doi:10.1175/JPO2985.1.

Jansen, M. F., and I. M. Held (2014), Parameterizing subgrid-scale eddy effects using energetically consistent backscatter, *Ocean Modell.*, *80*, 36–48, doi:10.1016/j.ocemod.2014.06.002.

Karsten, R., and J. Marshall (2002), Constructing the residual circulation of the ACC from observations, *J. Phys. Oceanogr.*, *32*, 3315–3327.

Khatiwala, S., F. Primeau, and T. Hall (2009), Reconstruction of the history of anthropogenic CO_2 concentrations in the ocean, *Nature*, *462*, 346–350, doi:10.1038/nature08526.

Kjellsson, J., P. R. Holland, G. J. Marshall, P. Mathiot, Y. Aksenov, A. C. Coward, S. Bacon, A. P. Megann, and J. Ridley (2015), Model sensitivity of the Weddell and Ross seas, Antarctica, to vertical mixing and freshwater forcing, *Ocean Modell.*, *94*(C), 141–152, doi:10.1016/j.ocemod.2015.08.003.

Large, W., J. Mcwilliams, and S. Doney (1994), Oceanic vertical mixing: A review and a model with a nonlocal boundary layer parameterization, *Rev. Geophys.*, *32*(4), 363–403.

Liu, L., and R. Huang (2012), The global subduction/obduction rates: Their interannual and decadal variability, *J Clim.*, *25*, 1096–1115, doi:10.1175/2011JCLI4228.1.

Lumpkin, R., and K. Speer (2007), Global ocean meridional overturning, *J. Phys. Oceanogr.*, *37*, 2550–2562, doi:10.1175/JPO3130.1.

Luyten, J., J. Pedlosky, and H. Stommel (1983), The ventilated thermocline, *J. Phys. Oceanogr.*, *13*(2), 292–309.

Marshall, J., C. Hill, L. Perelman, and A. Adcroft (1997a), Hydrostatic, quasi-hydrostatic, and nonhydrostatic ocean modeling, *J. Geophys. Res.*, *102*(C3), 5733–5752.

Marshall, J., A. Adcroft, C. Hill, and L. Perelman (1997b), A finite-volume, incompressible Navier Stokes model for studies of the ocean on parallel computers, *J. Geophys. Res.*, *102*(C3), 5753–5766.

Mazloff, M., P. Heimbach, and C. Wunsch (2010), An eddy-permitting Southern Ocean state estimate, *J. Phys. Oceanogr.*, *40*, 880–899, doi:10.1175/2009JPO4236.1.

McCartney, M. S. (1977), Subantarctic Mode Water, in *A Voyage of Discovery: George Deacon 70th Anniversary Volume,* edited by M. V. Angel, pp. 103–119, Supplement to Deep-Sea Research, Pergamon Press, Oxford.

McDougall, T. J. (1989), Streamfunctions for the lateral velocity vector in a compressible ocean, *J. Mar. Res.*, *47*, 267–284.

McNeil, B., B. Tilbrook, and R. Matear (2001), Accumulation and uptake of anthropogenic CO_2 in the Southern Ocean, south of Australia between 1968 and 1996, *J. Geophys. Res.*, *106*(C12), 31,431–31,445, doi:10.1029/2000JC000331.

Musgrave, D. (1990), Numerical studies of tritium and helium-3 in the thermocline, *J. Phys. Oceanogr.*, *20*, 344–373.

Pedlosky, J. (1984), Cross-gyre ventilation of the subtropical gyre: An internal mode in the ventilated thermocline, *J. Phys. Oceanogr.*, *14*, 1172–1178.

Primeau, F., and M. Holzer (2006), The ocean's memory of the atmosphere: Residence-time and ventilation-rate distributions of water masses, *J. Phys. Oceanogr.*, *36*, 1439–1456.

Qu, T., S. Gao, and R. A. Fine (2013), Subduction of south pacific tropical water and its equatorward pathways as shown by a simulated passive tracer, *J. Phys. Oceanogr.*, *43*(8), 1551–1565, doi:10.1175/JPO-D-12-0180.1.

Rintoul, S., C. Hughes, and D. Olbers (2001), The Antarctic Circumpolar Current system, in *Ocean Circulation and Climate*, edited by G. Siedler and J. Church, pp. 271–302, Int. Geophys. Ser., Academic Press.

Robinson, A., and H. Stommel (1959), The oceanic thermocline and the associated thermohaline circulation, *Tellus, 11*(3), 295–308.

Sabine, C., et al. (2004), The oceanic sink for anthropogenic CO_2, *Science*, *305*, 367–371, doi:10.1126/science.1097403.

Sallée, J., and S. Rintoul (2011), Parameterization of eddy-induced subduction in the Southern Ocean surface-layer, *Ocean Modell.*, *39*, 146–153, doi:10.1016/j.ocemod.2011.04.001.

Sallée, J., K. Speer, and R. Morrow (2008a), Response of the Antarctic Circumpolar Current to atmospheric variability, *J Clim.*, *21*, 3020–3039, doi:10.1175/2007JCLI1702.1.

Sallée, J., R. Morrow, and K. Speer (2008b), Eddy heat diffusion and subantarctic mode water formation, *Geophys. Res. Lett.*, *35*, L05607, doi:10.1029/2007GL032827.

Sallée, J., K. Speer, S. Rintoul, and S. Wijffels (2010), Southern Ocean thermocline ventilation, *J. Phys. Oceanogr.*, *40*, 509–529, doi:10.1175/2009JPO4291.1.

Sallée, J.-B., R. J. Matear, S. R. Rintoul, and A. Lenton (2012), Localized subduction of anthropogenic carbon dioxide in the Southern Hemisphere oceans, *Nat. Geosci.*, *5*(8), 579–584, doi:10.1038/ngeo1523.

Sarmiento, J., N. Gruber, M. Brzezinski, and J. Dunne (2004), High-latitude controls of thermocline nutrients and low latitude biological productivity, *Nature*, *427*(6969), 56–60.

Schopp, R., and M. Arhan (1986), A ventilated middepth circulation model for the eastern north Atlantic, *J. Phys. Oceanogr.*, *16*, 344–357.

Sloyan, B., and S. Rintoul (2001), Circulation, renewal, and modification of Antarctic mode and intermediate water*, *J. Phys. Oceanogr.*, *31*, 1005–1030.

Speer, K., and E. Tziperman (1992), Rates of water mass formation in the north Atlantic Ocean, *J. Phys. Oceanogr.*, *22*, 93–104.

Speer, K., S. Rintoul, and B. Sloyan (2000), The diabatic Deacon cell, *J. Phys. Oceanogr.*, *30*(12), 3212–3222.

Stark, S., R. Wood, and H. Banks (2006), Reevaluating the causes of observed changes in Indian Ocean water masses, *J Clim.*, *19*, 4075–4086.

Stossel, A., D. Notz, F. A. Haumann, H. Haak, J. Jungclaus, and U. Mikolajewicz (2015), Controlling high-latitude Southern Ocean convection in climate models, *Ocean Modell.*, *86*(C), 58–75, doi:10.1016/j.ocemod.2014.11.008.

Talley, L. (2008), Freshwater transport estimates and the global overturning circulation: Shallow, deep and throughflow components, *Prog. Oceanogr.*, *78*(3), 257–303, doi:10.1016/j.pocean.2008.05.001.

Talley, L. (2013), Closure of the global overturning circulation through the Indian, Pacific, and Southern Oceans: Schematics and transports, *Oceanography*, *26*(1), 80–97, doi:10.5670/oceanog.2013.07.

Talley, L., et al. (2016), Changes in ocean heat, carbon content, and ventilation: A review of the first decade of GO-SHIP global repeat hydrography, *Annu. Rev. Mar. Sci.*, *8*(1), 185–215, doi:10.1146/annurev-marine-052915-100829.

Thompson, A. (2008), The atmospheric ocean: Eddies and jets in the Antarctic Circumpolar Current, *Philos. Trans. R. Soc. A*, *366*, 4529–4541, doi:10.1098/rsta.2008.0196.

Timmermann, R., and A. Beckmann (2004), Parameterization of vertical mixing in the Weddell sea, *Ocean Modell.*, *6*(1), 83–100, doi:10.1016/S1463-5003(02)00061-6.

Timmermann, R., and M. Losch (2005), Using the Mellor–Yamada mixing scheme in seasonally ice-covered seas—corrigendum to: Parameterization of vertical mixing in the Weddell sea [ocean modelling 6 (2004) 83–100], *Ocean Modell.*, *10*(3–4), 369–372, doi:10.1016/j.ocemod.2004.11.001.

Trossman, D. S., L. Thompson, S. Mecking, and M. J. Warner (2012), On the formation, ventilation, and erosion of mode waters in the north Atlantic and Southern Oceans, *J. Geophys. Res.*, *117*, C09026, doi:10.1029/2012JC008090.

Wang, J., M. R. Mazloff, and S. T. Gille (2014), Pathways of the Agulhas waters poleward of 29 °S, *J. Geophys. Res. Oceans*, *119*, 4234–4250, doi:10.1002/2014JC010049.

Waterhouse, A. F., et al. (2014), Global patterns of diapycnal mixing from measurements of the turbulent dissipation rate, *J. Phys. Oceanogr.*, *44*(7), 1854–1872.

Welander, P. (1959), An advective model of the ocean thermocline, *Tellus*, *11*(3), 309–318, doi:10.1111/j.2153-3490.1959.tb00036.x.

Whalen, C. B., J. A. MacKinnon, L. D. Talley, and A. F. Waterhouse (2015), Estimating the mean diapycnal mixing using a finescale strain parameterization, *J. Phys. Oceanogr.*, *45*(4), 1174–1188, doi:10.1175/JPO-D-14-0167.1.

Whitworth, T. (1983), Monitoring the transport of the Antarctic Circumpolar Current at Drake Passage, *J. Phys. Oceanogr.*, *13*, 2045–2057.

Whitworth, T., and R. Peterson (1985), Volume transport of the Antarctic Circumpolar Current from bottom pressure measurements, *J. Phys. Oceanogr.*, *15*, 810–816.

Erratum

In the originally published version of this manuscript, there were errors in Figure 5 and its caption. The figure caption should have been published as: Cunningham geostrophic streamfunction (1 Sv = 10^6 m^3/s), derived from annual mean temperature and salinity data using the Gibbs Seawater Toolbox (GSW), with respect to 1000 dbar on several density surfaces between 30.8–31.8 kg/m^3 (*Cunningham*, 2000). The two solid lines are the 90 Sv and 130 Sv contours of the annual mean barotropic streamfunction.

In addition to the change to Figure 5, the following reference has been added: Cunningham, S. A. (2000), Circulation and volume flux of the North Atlantic using synoptic hydrographic data in a Bernoulli inverse, *J. Marine Res., 58,* 1–35. In addition, the reference "Montgomery, R. (1937), A suggested method for representing gradient flow in isentropic surfaces, *Bulletin of the American Meteorological Society, 18 (210)*" has been removed.